HHS Public Access

Author manuscript

J Comp Neurol. Author manuscript; available in PMC 2020 November 01.

Published in final edited form as:

J Comp Neurol. 2019 November 01; 527(16): 2675–2693. doi:10.1002/cne.24699.

Domain-specific distribution of gap junctions defines cellular coupling to establish a vascular relay in the retina

Elena Ivanova, **Tamas Kovacs-Oller**, **Botir T Sagdullaev**

Burke Neurological Institute at Weill Cornell Medicine, White Plains, NY 10605.

Abstract

In the retina, diverse functions of neuronal gap junctions (GJs) have been established. However, the distribution and function of vascular GJs are less clear. Here in the mouse retina whole mounts, we combined structural immunohistochemical analysis and a functional assessment of cellular coupling with a GJ-permeable tracer Neurobiotin to determine distribution patterns of three major vascular connexins. We found that Cx43 was expressed in punctate fashion on astroglia, surrounding all types of blood vessels and in continuous string-like structures along endothelial cell contacts in specialized regions of the vascular tree. Specifically, these Cx43-positive strings originated at the finest capillaries and extended towards the feeding artery. Since this structural arrangement promoted strong and exclusive coupling of pericytes and endothelial cells along the corresponding branch, we termed this region a “vascular relay”. Cx40 expression was found predominantly along the endothelial cell contacts of the primary arteries and did not overlap with Cx43-positive strings. At their occupied territories, Cx43 and Cx40 clustered with tight junctions and, to a lesser extent, with adhesion contacts, both key elements of the blood-retina barrier. Finally, Cx37 puncta were associated with the entire surface of both mural and endothelial cells across all regions of the vascular tree. This combinatorial analysis of vascular connexins and identification of the vascular relay region will serve as a structural foundation for future studies of neurovascular signaling in health and disease.

Graphical Abstract

Corresponding Authors: Botir T. Sagdullaev or Elena Ivanova, 785 Mamaroneck Ave., White Plains, NY 10605, bos2005@med.cornell.edu or eli3001@med.cornell.edu.

Data Availability Statement:

The data that support the findings of this study are available from the corresponding author upon reasonable request.

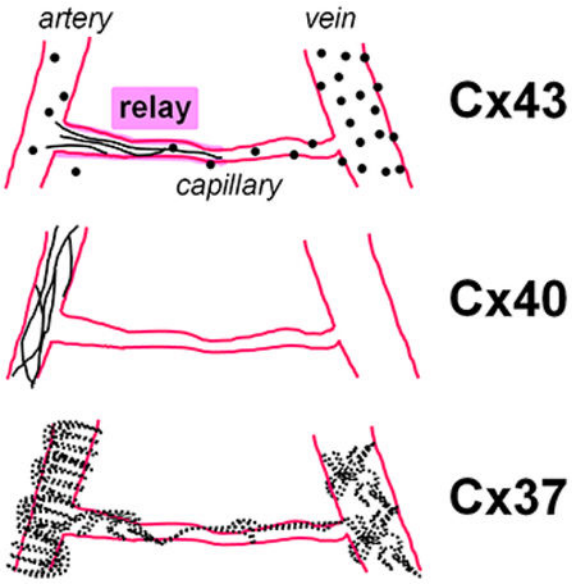

In the mouse retina vasculature we have determined connexins' distribution and cellular coupling. Cx43 strings connected capillaries with the feeding artery and promoted coupling. We termed this region a "vascular relay". Cx40 expression was in primary arteries. Cx37 puncta were on majority of vascular cells.

Keywords

endothelial cell; pericyte; gap junctions; cell coupling; vascular relay; RRID:IMSR_JAX:000664; RRID:IMSR_JAX:008241; RRID: SCR_003070; RRID:SCR_003210; RRID:SCR_003210; RRID:AB_67122; RRID:AB_2532189; RRID:AB_476857; RRID:AB_10917597; RRID:AB_2340916; RRID:AB_2722598; RRID:AB_262054; RRID:AB_177521; RRID:AB_2161028

Introduction

Gap junctions (GJs) are transmembrane channels which enable direct electrical communication (Furshpan & Potter, 1957; Watanabe, 1958; Weidmann, 1969) and metabolite exchange between cells (Gilula, Reeves, & Steinbach, 1972; Pitts & Simms, 1977). Around twenty different connexin proteins, the building blocks of the GJs, have been identified in humans and rodents (Sohl & Willecke, 2004). Six connexins form a hemichannel, and two opposing hemichannels of adjacent cells establish a functional GJ (Makowski, Caspar, Phillips, & Goodenough, 1977). Different connexin subunits confer distinct functional properties to GJs, including pore size, voltage dependence, and sensitivity to modulators, both intra- and extracellular (Sohl & Willecke, 2004). Therefore, knowledge of connexin composition and their assignment to specific cell types is needed to understand their physiological role.

In the retina, diverse functions of neuronal GJs have been well documented (for review see Volgyi, Kovacs-Oller, Atlasz, Wilhelm, & Gabriel, 2013). They are involved in adaptation to

dark and light (Bloomfield, Xin, & Osborne, 1997; Tornqvist, Yang, & Dowling, 1988), circadian rhythms (Ribelayga, Cao, & Mangel, 2008), development (Meister, Wong, Baylor, & Shatz, 1991), signaling along the rod and cone pathways (Deans, Volgyi, Goodenough, Bloomfield, & Paul, 2002; Schneeweis & Schnapf, 1995), and synchronized cells firing (Brivanlou, Warland, & Meister, 1998; Mastronarde, 1983). GJs were also shown to play a central role in retinal pathological processes, including propagation of the “death signal” in photoreceptor degeneration (Ripps, 2002), glaucoma (Akopian et al., 2014) and aberrant neuronal excitability in retinal degenerations (Ivanova, Yee, Baldoni, & Sagdullaev, 2016; Toychiev, Ivanova, Yee, & Sagdullaev, 2013). The roles of diverse GJs in vasculature are less established. In the retina, blood vessels are composed of arteries, veins, and capillaries. They occupy four distinct vascular layers, creating spatially and functionally specialized domains of the vascular tree (Fig. 1a). In this tree, a deep vascular layer serves the outer plexiform layer, while intermediate and sublaminar capillary layers nourish the inner plexiform layer (Ivanova, Toychiev, Yee, & Sagdullaev, 2014). Here, a close proximity to neuronal synapses enables capillaries to sense neuronal activity and adjust blood flow on demand (Kornfield & Newman, 2014). The retinal arterioles are positioned outside of the synaptic nets, in the superficial layer. In contrast to other parts of the brain, they are not directly exposed to the neurotransmitters and depend on a “sensory” input from the capillaries. The underlying structures mediating this interaction along the vascular tree remains unclear. This knowledge is of particular importance in the retina, where the vasculature lacks central regulation and must rely on local signals (Delaey & Van De Voorde, 2000). Indeed, direct electrical communication between vascular cells via GJs has been shown to control vasomotor tone and propagation of vasomotor response in the retina (Ivanova, Kovacs-Oller, & Sagdullaev, 2017). GJs were also shown to play a role in vascular pathology. In diabetic retinopathy, downregulation of GJs expression exacerbated vascular leakage (Bobbie et al., 2010; Li, Sato, Haimovici, Okamoto, & Roy, 2003; Oku, Kodama, Sakagami, & Puro, 2001; Tien, Muto, Barrette, Challyandra, & Roy, 2014), indicating a role for GJs in the maintenance of blood-retina barrier.

The types of vascular connexins, their distribution, and functions in specialized vascular domains are not clear. Among vascular GJs, several types of connexins have been identified in the heart and parts of the CNS: Cx37, Cx40, Cx43, and Cx45 (Delorme et al., 1997; Haefliger, Nicod, & Meda, 2004). To determine subunit composition and distribution of GJs in the retina, we labeled retina whole mounts of Ng2-DsRed mice for Cx37, Cx40, and Cx43. Once specific patterns of connexins’ distribution along the vascular tree have been determined, we utilized a selective GJ-permeable tracing assay to determine their role in cell-to-cell communications.

Methods

Animals.

All animal procedures were performed in accordance to the Institutional Animal Care and Use Committee of Weill Cornell Medicine, and in accordance with the National Institutes of Health *Guide for the care and use of laboratory animals*. Wildtype mice (The Jackson Laboratory, stock #000664, RRID:IMSR_JAX:000664) and mice with contractile vascular

cells expressing red fluorescent protein (NG2-DsRed, The Jackson Laboratory, Tg(Cspg4-DsRed.T1)1Akik/J, stock #008241, RRID:IMSR_JAX:008241) of either sex were used at the age between p60 and p120.

Whole mount retina preparation for in vitro recordings.

After the animal was killed, its eyes were enucleated and placed in bicarbonate-buffered Ames solution, constantly equilibrated with 95% O2 and 5% CO2. All our measurements have been made under consistent O2 levels across all experimental conditions. The cornea, iris, and lens were removed. The retina was dissected into four equal quadrants. Quadrants were placed photoreceptor surface down on a modified Biopore Millicell filter (Millipore). This preparation was transferred to a recording chamber on the stage of an upright Nikon FN1 microscope equipped with Hoffman modulation contrast optics (Modulation Optics) and bathed (1 ml/min) with bicarbonate-buffered Ames solution (Sigma, A1420). Pharmacological agents were added to this solution at a final concentration indicated in the text. All experiments were performed at a near physiological temperature of 32°C.

Vasomotor response assessment.

The detailed protocol for vasomotor response assessment has been recently published (Ivanova et al., 2017). In the retina whole mount, identified pericytes were targeted on capillaries in the superficial vascular layer, avoiding those located on arterioles and veins. Capillaries were defined based on several morphological criteria: (1) diameter not exceeding 10 μm, approximately equivalent to the diameter of red blood cells, which are readily present in the living tissue; (2) lack of a smooth muscle actin; and (3) presence of clearly visible pericytes. In the experiments, we targeted fluorescently labeled pericytes in NG2-DsRed mice. In genetically unmodified mice, we were able to identify pericytes in contrast optics based on their characteristic appearance on the abluminal side of the vessel wall (Kawamura et al., 2003). Pericytes were focally stimulated by a current pulse (3–10 μA, 2 ms; Grass Technologies) using an electrode filled with HEPES-buffered extracellular Ringer's solution, containing the following (in mM): 137 NaCl, 2.5 KCl, 2.5 CaCl2, 1.0 MgCl2, 10 Na-HEPES, 28 glucose, pH 7.4. Electrodes were pulled from borosilicate glass (WPI, 1B150F-4) with a P-97 Flaming/Brown puller (Sutter Instruments, Novato, CA) and had a measured resistance of ~5 MΩ. For consistency across all experiments, the electrode was placed near the cell body of the targeted pericyte. Responses to stimuli were captured on video or time-lapse photo with a microscope-mounted Sony A7s full frame camera. The focus of the image was continually kept on capillary lumen aided by live image projection onto an external HDMI monitor.

Neurobiotin tracing.

Electrodes were pulled from borosilicate glass (1B150F-4) with a P-97 Flaming/Brown puller and had a resistance of ~1–2 MΩ. As a first step, pipette was filled with filtered Ames solution supplemented with 100 μg/ml papain (~1 Unit/ml). The papain-containing solution was applied for 5 min to dissolve the vascular basement membrane covering pericytes. Second, a fresh pipette was filled with intracellular solution containing (in mM): 120 Cs-gluconate, 10 tetraethylammonium chloride (TEA-Cl), 1.0 CaCl2, 1.0 MgCl2, 11 ethylene glycol-bis(beta-aminoethyl ether)-N,N,N',N'- tetraacetic acid (EGTA), and 10 sodium N-2-

hydroxyethylpiperazine-N'−2-ethanesulfonic acid (Na-HEPES), adjusted to pH 7.2 with CsOH. The solution was supplemented with 2% Neurobiotin (Vector, SP-1120) and 0.5% Alexa488-hydrazide (ThermoFischer Scientific, A10436). This new pipette was pressed against the cleaned pericyte to establish a direct contact between the pipette and the pericyte. Next, the membrane of the pericyte was gently pulled inside the pipette. The alternating voltage steps between −300 mV and +50 mV, 2 Hz, were applied for 1 min to confirm successful targeting of a pericyte after filling with Alexa488-hydrazide. If the pericyte was revealed by Alexa488 labeling, Neurobiotin was electroporated by 3 min of +200 mV −50 mV, 2 Hz voltage steps. If the targeted pericyte was not filled with Alexa488 it was abandoned. After Neurobiotin electroporation, the sample was left for 15 min to allow Neurobiotin diffusion. Next, the sample was fixed in a fixative containing: 4% carbodiimide and 0.25% paraformaldehyde in 0.1 M phosphate saline (PBS, pH = 7.3) for 15 min at room temperature. All electroporations were made with MultiClamp 700B patch-clamp amplifier (Molecular Devices, Sunnyvale, CA) using Signal software (CED, UK).

Antibodies and other reagents.

All primary antibodies are listed in Table 1.

Albumin antibody.

To remove cross reactive antibodies, antiserum to mouse albumin was cross absorbed using bovine, human and pig immuno-sorbents. The antibody to mouse albumin was isolated by affinity chromatography using antigen-coupled agarose beads. By immunoelectrophoresis and ELISA this antibody reacts specifically with mouse albumin (manufacturer information). Less than 2% cross reactivity to bovine, human and pig albumin was detected. The specificity of the antibodies was determined in cultural primary mouse hepatocytes under control conditions and conditions when albumin synthesis was blocked (Guo, Xu, Lu, & Xie, 2017). In the retina, the staining for albumin was contained inside retinal blood vessels which correspond to the location of the blood plasma albumin (our data; Iwase et al., 2013).

Claudin5 antibody.

Reactivity has been confirmed with rat, human and mouse claudin5 using rat lung, mouse kidney, mouse small intestine, mouse lung homogenates, human colon tissue, and CACO-2 human cell line. This antibody reacts specifically with the ~ 22–24 kDa endogenous claudin5 protein (manufacturer information). In the retina, it labeled endothelial cells (Yanagida et al., 2017) similar to a different antibody which was validated in control and claudin5 RNAi-treated retinas (rabbit anti-claudin5 (Zymed); Campbell et al., 2009).

Connexin 43 antibody from Sigma (Cx43s, Sigma, #C6219).

Polyclonal antibody against Cx43 was produced against a synthetic peptide corresponding to the C-terminal segment of the cytoplasmic domain (amino acids 363–382 with N-terminal added lysine) of human/rat Cx43. The antibody specificity was confirmed by Western blot and immunocytochemistry in human and rodent retina (Danesh-Meyer et al., 2012; Kerr et al., 2010). This antibody specificity was also confirmed by immunocytochemistry and

Western blot comparison of heart tissue from *wt* and *Cx43* KO mice (Denuc et al., 2016). This antibody is included in Validated Antibody Database (https://www.labome.com/knockout-validated-antibodies/Cx43-antibody-knockout-validation-Sigma-Aldrich-C6219.html).

Connexin 43 antibody from Alomone (Cx43a, Alomone, #ACC-201).

Polyclonal antibody against Cx43 was produced against a synthetic peptide corresponding to the C-terminal segment of the cytoplasmic domain (amino acids 331–345) of human Cx43. Rat - 14/15 amino acid residues identical; mouse - 13/15 amino acid residues identical. The antibody specificity was confirmed by Western blot in mouse brain membranes and rat heart membranes; preincubation with control peptide antigen eliminated the band (manufacturer information). In our hands, the antibody produced identical patterns in the mouse retina whole mount (compare Fig. 2j, k with Fig. 2n, o) as a different Cx43 antibody (Sigma, #C6219, characterized above). These antibodies were raised against different non-overlapping epitopes. In addition, when the Alomone's Cx43 antibody was preincubated with the control peptide antigen, the staining in the mouse retina was eliminated (Fig. 2p).

Connexin 37 polyclonal antibody was raised in rabbit against (C)EHQMAKISVAEDGR peptide, corresponding to amino acid residues 131–144 of rat Cx37 intracellular loop. The mouse Cx37 has the identical sequence. The sequence of the peptide was confirmed by amino acid analysis and mass spectrometry. This antibody was tested using a Western blot in mouse heart and lung lysate along with the negative control where the same tissue was preincubated with the control peptide antigen (manufacturer information). When the antibody was preabsorbed with the control peptide provided by the manufacturer, the staining in the retina was eliminated (Fig. 2). Antibody produced similar staining in vascular endothelial cells as a different antibody against Cx37 (Anti-Cx37, David Paul, Harvard Medical School; Gabriels & Paul, 1998).

Connexin 40 antibody was produced against intracellular, C-terminus peptide (C)GHRFPQGYHSDKR, corresponding to amino acid residues 328–340 of rat Connexin-40. The mouse sequence has 12 out of 13 amino acid identical residues. The antibody was validated by Western blot analysis of rat and mouse heart lysates in parallel with the lysate incubated with control peptide antigen (manufacturer information). We confirmed the specificity of the antibody by eliminating labeling in the retina after preabsorption of the antibody with a control peptide (Fig. 2). The labeling was similar to the pattern observed with a different antibody in the developing mouse retina (rabbit polyclonal antibody against Cx40, Alpha Diagnostic International, Cx40-A; (Haefliger et al., 2017)).

SMA antibody.

The antibody recognizes single isoform of α-smooth muscle actin in rabbit, guinea pig, mouse, chicken, snake, sheep, goat, human, frog, rat, canine, and bovine. The antibody was tested in Western blot and in immunolabeling of smooth muscle cells from bovine aortas using the monoclonal anti-ACTA2 antibody (manufacturer information). In the rat retina, the antibody labeled arteries and the pattern was comparable with the labeling produced by two different antibodies (FITC-conjugated goat anti-mouse IgG2a (Southern Biotechnology

Associates) and Texas red– conjugated sheep anti-mouse Ig (Amersham); Hughes & Chan-Ling, 2004).

CD31/PECAM-1. Detects mouse CD31/PECAM-1 in direct ELISAs and Western blots (band ~130 kDa). In direct ELISAs and Western blots, approximately 10% cross-reactivity with recombinant human CD31 and recombinant porcine CD31 is observed. Detected mouse CD31 and rat CD31 in flow cytometry (manufacturer information). In the retina, the antibody stained vascular endothelial cells (Fang et al., 2017; Wilhelm et al., 2016).

GFAP antibody.

Reacts with both native and recombinant protein of human, mouse, rat, bovine and pig. The antibody stained sharply defined cytoplasmic filaments of astroglia cells in tissue culture. It also stained processes of astrocytes in sections of brain tissues. In the Western blot analysis, the antibody revealed a band of 55 kDa (manufacturer information). In the mouse retina, the antibody produced an identical pattern of astroglia labeling as a different GFAP antibody (Cell Signalling, Cat.# 12389; our data).

Secondary antibodies were conjugated to Alexa 488 (1:1000; green fluorescence, Molecular Probes), Alexa 568 (1:1000; red fluorescence, Molecular Probes), Alexa 647 (1:400; far red fluorescence, Molecular probes), or Cy5 (1:500; far red fluorescence, Jackson ImmunoResearch).

Immunohistochemistry.

As described previously (Ivanova, Toychiev, Yee, & Sagdullaev, 2013), following euthanasia, the eyes were removed and placed in bicarbonate-buffered Ames' medium (Sigma Aldrich, St Louis, MO) equilibrated with 95% O2 and 5% CO2. The cornea was removed by an encircling cut above *ora serrata*, and the iris, lens, and vitreous were extracted. The remaining eyecup, with the retina still attached to the pigment epithelium, was submersion-fixed on a shaker in freshly prepared 4% carbodiimide with 0.25% paraformaldehyde in 0.1 M phosphate saline (PBS, pH = 7.3) for 15 min at room temperature. After fixation, the eye cups were washed in PBS for 2 h and the retinas were detached from the eye-cups. Isolated retinas were blocked for 10 h in a PBS solution containing 5% Chemiblocker (membrane-blocking agent, Chemicon), 0.5% Triton X-100, and 0.05% sodium azide (Sigma). Primary antibodies were diluted in the same solution and applied for 72 h, followed by incubation for 48 h in the appropriate secondary antibody. In multi-labeling experiments, tissue was incubated in a mixture of primary antibodies, followed by a mixture of secondary antibodies. All steps were completed at room temperature. After staining, the tissue was flat-mounted on a slide, ganglion cell layer up, and coverslipped using Vectashield mounting medium (H-1000, Vector Laboratories). The coverslip was sealed in place with nail polish. To avoid extensive squeezing and damage to the retina, small pieces of a broken glass cover slip (Number 1 size) were placed in the space between the slide and the coverslip.

Antibody validation.

To optimize tissue fixation, we tested 4% paraformaldehyde, 4% carbodiimide, and a combination of 0.25% paraformaldehyde with 4% carbodiimide with all connexin antibodies (Fig. 2). A combination of 0.25% paraformaldehyde with 4% carbodiimide was chosen for optimal labeling and antibody validation. All connexin antibodies from Alomone came with control peptides. The pre-absorption was conducted according to manufacturer's protocol by mixing primary antibody with the correspondent control peptides (1–2 μg peptide per 1 μg antibody) for 3 h on a shaker. The mixture was applied to halves of retina whole mounts. For positive controls, the remaining retinal halves were incubated with primary antibodies without control peptides. In an additional control, retina whole mount was incubated with secondary antibody alone (Fig. 2l).

Quantification of retinal vasculature and connexin distribution.

All data were analyzed in ImageJ (http://imagej.nih.gov/ij/, RRID: SCR_003070). Arteries were distinguished from veins by smaller diameter and by a capillary-free zone around them. Identification was confirmed by immunostaining for smooth muscle actin. Z-stacks images of retinas were taken with a 10x air, 20x water, 60x oil, and 100x oil objectives (Nikon) starting from the lowest magnification. To quantify the densities of connexins, 60x images of connexins were first thresholded and the total sum of connexin-positive areas was calculated as a percentage of either the blood vessel (Fig. 4d, 4e, 7e, and 9e) or the entire area (Fig. 4h, 7g, and 9g). Specifically, we used 212 μm × 212 μm areas to determine the densities of connexins and each data point for the cluster analysis represents a segment of a blood vessel within this area (Fig. 4d and 4e). Vertical views were generated by 90 degree rotation of confocal z-stacks.

Cluster analysis.

Cluster analysis was performed using Statistica software (StatSoft, Inc., Tulsa, OK, USA) on two parameters: density of connexin-positive strings and density of connexin positive puncta. Two distinct methods of cluster analysis were chosen: K-means (Kong, Fish, Rockhill, & Masland, 2005) and hierarchical clustering (Coombs, van der List, Wang, & Chalupa, 2006). For K-means analysis, we used initially predetermined six clusters, which is equal to the number of blood vessel types: artery, vein, capillary, relay and non-vascular. The analysis then maximized the distances between each cluster while minimizing the differences between the members within a single cluster. The hierarchical clustering does not require a predetermined number of clusters. This analysis begins by treating each member as its own individual cluster, and the clusters are then grouped together based on similarities across the defined parameters. The final result produces a dendrogram, where two cells with greater similarity are linked together at a lower linkage distance.

Statistical analysis.

Statistical analysis was performed in either SPSS v.19 (IBM, RRID:SCR_003210) or SigmaPlot v.11 (Systat, RRID:SCR_003210), using t-test. For multiple comparisons, analysis of variance (ANOVA) with post-hoc Tukey's test or repeated-measures ANOVA was used. The data are presented as mean ± standard error, unless otherwise indicated. The

number of samples (n) indicates number of animals per group. To avoid introduction of non-independent data into statistical analysis, first, multiple samples from individual animals were averaged within subject, then the data between animals were compared (Aarts, Verhage, Veenvliet, Dolan, & van der Sluis, 2014).

Data Availability Statement.

The data that support the findings of this study are available from the corresponding author upon reasonable request.

Results

A network of coupled vascular cells mediate vasomotor response.

To assess GJ-mediated coupling between vascular cells and its role in the vasomotor response, we used living retina whole mounts from NG2-DsRed mice. In these mice, DsRed fluorescent protein was expressed in all mural cells (Fig. 1c, Schallek, Geng, Nguyen, & Williams, 2013), including pericytes and smooth muscle cells. For single-cell Neurobiotin tracer injections, we targeted individual pericytes from capillary regions, distinguished by the absence of smooth muscle actin (SMA) labeling. Using a patch-clamp pipette, an individual pericyte was electroporated and infused with Neurobiotin for 20 minutes, which was experimentally determined not to damage the target cell and to allow for Neurobiotin to spread to its GJ-coupled neighbors (Bloomfield et al., 1997; Kothmann, Massey, & O'Brien, 2009; Fig. 1c, green labeling, arrow marks the targeted pericyte, see Methods). Under control conditions, Neurobiotin spread along the vascular network from the injected pericyte towards the artery and, to a lesser extent, towards the vein (Fig. 1e). Interestingly, Neurobiotin staining was limited to vascular cells - pericytes and endothelial cells. In the presence of a pan-GJ blocker meclofenamic acid (MFA, 50 μM), the Neurobiotin labeling was restricted exclusively to the injected pericyte. This data confirms that a) only a single targeted pericyte was initially loaded with Neurobiotin, and that b) its spread occurred through direct GJ-mediated connections between the neighboring vascular cells, thus excluding the possibility for nonspecific tracer diffusion (Fig. 1d–e, MFA).

In response to a neuronal signal, blood vessels either constrict or dilate. The vasomotor response engages a number of adjacent pericytes. However, whether it is mediated by a direct GJ-mediated coupling is not clear. To further address the role of GJs in vasomotor response, we directly stimulated an individual pericyte and measured the change in the vascular diameter and its propagation (Fig. 1f). This approach enables targeted, reproducible induction and assessment of vasomotor response. Under control conditions, depolarization of a targeted pericyte led to constriction of the capillary directly under the stimulated pericyte, as well as beyond its boundary in the neighboring vascular regions (Fig. 1g and i). When GJs were blocked by 50 μM MFA, the constriction of the targeted pericyte was not affected, however, it did not spread to the neighboring regions (Fig. 1h and i). Thus, GJs are required for vascular cell coupling and the vasomotor response propagation.

Connexins 37, 40, and 43 are concentrated on the retinal vasculature.

To determine the subunit distribution of vascular GJs in the retina and their relationship to vascular elements, we tested a variety of antibodies against vascular connexins identified in the heart and brain (Brisset, Isakson, & Kwak, 2009; Gros & Jongsma, 1996; Haefliger et al., 2004). In these tissues, Cx37, Cx40, Cx43 were localized in the vasculature, making them primary candidates for vascular GJs in the retina. Figure 2 validates Cx37, Cx40, and Cx43 antibodies in retina whole mounts. Blood vessels were visualized by labeling for platelet endothelial cell adhesion molecule-1 (PECAM-1), an established marker of vascular endothelial cells (Fig. 2, blue). Three different fixatives were used: common 4% paraformaldehyde; 4% carbodiimide, a superior fixative for synaptic proteins (Csaba, Kovacs, & Pallinger, 2006; Fletcher, Hack, Brandstatter, & Wassle, 2000; Gastinger, O'Brien, Larsen, & Marshak, 1999; Haverkamp & Wassle, 2000; Ivanova et al., 2013; Koulen, Fletcher, Craven, Bredt, & Wassle, 1998); and an optimized combination of both (4% carbodiimide and 0.25% PFA). The performance of each antibody was evaluated by comparing signal to background ratios and is summarized in Fig. 2t. Overall, all antibodies against connexins performed better in 4% carbodiimide fixed tissue (Fig. 2b, f, j and n), revealing more vascular-specific structures and less background noise. However, this fixative was ineffective in preservation of Neurobiotin and DsRed (Fig. 2r), and the fixed tissue remained fragile and difficult to handle. The optimized combination of the fixatives (4% carbodiimide and 0.25% PFA) was effective in preserving of all targets, minimizing the background, and was used for the rest of the study (Fig. 2c, g, k, o and s).

Next, we tested the antibody specificity by pre-absorbing primary antibodies with control peptides provided by the manufacturer. This mixture was applied to halves of the retina whole mounts (Fig. 2d, h and p). The remaining tissue was incubated with the correspondent primary antibody without pre-absorption (Fig. 2c, g and o) or with secondary antibody alone (Fig. 2l). Labeling by anti-connexin antibodies was prevented by the correspondent control peptides confirming specificity of all anti-connexin antibodies in the current study. The widely used antibody to Cx43 from Sigma (Cx43s, Cat # C6219, Fig. 2i–k) did not have a control peptide and was validated by comparison with a different, less common, antibody to Cx43 from Alomone (Cx43a, Cat # ACC-201, Fig. 2m–p). In carbodiimide-based fixative, both antibodies produced an identical pattern. In 4% PFA, in contrast to puncta and string-like structures revealed by the Alomone antibody (Fig. 2m), the antibody from Sigma produced only punctate staining (Fig. 2i). Thus, Cx43 expression may be underestimated in the previous studies assessed with the antibody from Sigma in 4% PFA. All anti-connexin antibodies in the current study were produced in rabbit and could not be combined in the same specimen. Omission of all primary antibodies and application of the secondary anti-rabbit antibodies resulted in unrelated labeling of cells, likely microglia (Fig. 2l, arrow).

Outside of the blood vessels, many of the Cx-positive puncta were likely to be unspecific background (Fig. 3). In line with this conclusion, many of these random and evenly distributed puncta were present in pre-absorption experiments (Fig. 2). In some cases, however, the staining in the GCL was meaningful. Specifically, Cx37 was expressed on the membrane of a few RGC types (Fig. 3b, insert). This specific labeling was eliminated by pre-absorption with the control peptide (Fig. 2d). Both Cx40 and Cx43 labeling in GCL was

present in nuclei of different cell types (Fig. 3e and h). This labeling was also eliminated by antibody pre-absorption (Fig. 2h and p).

Furthermore, two different Cx43 antibodies labeled nuclei in the GCL, confirming their specificity. It is possible that Cx43 and Cx40 in the nuclei play distinct roles different from GJ function in these cells. Their C-terminals might serve as a transcriptional factor, as was shown in amphibian and mammal models (Dang, Doble, & Kardami, 2003; Kotini et al., 2018). Notably, both Cx43 and Cx40 antibodies were against the C-terminal and were localized to the nuclei. The antibody to Cx37 was raised against a sequence in one of the intracellular loops and the labeling was absent from the nucleus. Finally, we compared the levels of the Cx37, Cx40, and Cx43 expression in vasculature and surrounding neurons. To reveal the difference in the expression levels, the fluorescence intensity profiles were plotted (Fig. 3c, f and i) and intensity of the signal was compared between vasculature (blue) and neurons (red). All tested connexins had significantly higher expression in vascular cells, deeming them predominantly vascular connexins in the retina.

Differential expression of Cx43 along the vascular tree: identification of the “vascular relay” region.

To characterize the distribution of Cx43 in the retina, we used retina whole mounts of adult NG2-DsRed mice labeled for Cx43 and smooth muscle actin (SMA, Fig. 4). Low magnification imaging revealed close association of Cx43-labeling with all types of blood vessels. In high magnification images, bright punctate labeling was detected on major arteries and veins as well as on the capillaries (Fig. 4b). In addition to Cx43-positive puncta, string-like structures running along the blood vessels were detected in the regions of vascular tree connecting the finest capillaries to the feeding arteries (Fig. 4c). We hypothesized that these prominent strings of GJs at the transition between the capillaries and arteries are important for communication of vascular cells and termed this specialized part of the vascular tree as a “vascular relay”.

To further characterize the distinct features of Cx43 expression along the vascular tree, we determined the density of Cx43-positive puncta and strings for arteries, relays, capillaries, veins and non-vascular elements (area outside blood vessels, not associated with PECAM-1 labeling) and plotted corresponded densities for each location in a graph (Fig. 4d). In the graph, each data point represents a segment of the corresponding blood vessel. The individual samples of the same vascular region were clustered together and the clusters were well-separated from each other. The center of each cluster was determined by k-means cluster analysis (shown in black). When the same data were analyzed using a hierarchical clustering algorithm, which does not require knowledge of the number of clusters, the samples from the same vascular areas were again grouped together at a shorter linkage distances (Fig. 4e). This analysis confirms that the expression patterns of Cx43 were distinct along the vascular regions (Fig. 4f).

Next, we determined expression of Cx43 in the intermediate and deep vascular layers. These regions are predominantly occupied by the capillaries (Fig. 4g and h), and lacked large Cx43-positive puncta readily seen at the capillaries of the superficial layer. Interestingly, the Cx43-positive strings from relay regions in superficial layer continued uninterrupted into

some capillaries of the intermediate and deep layers. A distinct expression pattern of Cx43 in vascular regions prompted further analysis of Cx43 localization to specific members of the neurovascular unit. In retina whole mounts of NG2-DsRed mice labeled for Cx43 and SMA, we took high magnification confocal z-stacks (Fig. 5a–h). Each location was then analyzed in a horizontal plane (Fig. 5a, c, e and g), and in a vertical view, created by a 90 degree rotation of the z-stack segment (Fig. 5b, d, f and h). In all vascular regions, the puncta were not directly present on the vascular cells, as demonstrated by the intensity profiles (Fig. 5, non-overlapping maximums). This close association of puncta with blood vessels suggested their location on astrocytes, known to wrap their processes around vasculature. Indeed similar to findings of other laboratories (Guldenagel et al., 2000; Kuo, Chan-Ling, Wojcikiewicz, & Hill, 2008; Slavi et al., 2018), all puncta colocalized with the astrocytes labeled for glial fibrillary acidic protein (GFAP, Fig. 5i and j). In the vascular relay, Cx43-strings were located closer to the lumen of the blood vessels and were surrounded by mural cells (Fig. 5d). These strings were closely overlapping with PECAM-1, a selective marker for the endothelial cells (Fig. 5k–m). In addition to large Cx43-positive puncta located on the astrocytes and strings located on the endothelial cells, we detected additional small punctate labeling. While the precise location is not clear, these smaller plaques could be GJ formations between pericytes and endothelial cells, similar to ones observed using electron microscopy (Carlson, 1989; Durham, Dulmovits, Cronk, Sheets, & Herman, 2015).

Cx43 strings guide coupling of vascular cells along the vascular relay.

A unique pattern of Cx43 expression along the capillary-arteriolar vascular relay prompted a further investigation of this vascular region (Fig. 6). In the superficial vascular layer, the Cx43-positive strings have originated from the base of the secondary arterial branch populated by SMA-positive cells (Fig. 6a). The strings continued downstream into some (arrows), but not all capillaries of the intermediate and deep vascular layer (Fig. 6a–c, arrowheads). When we projected all vascular layers onto a single plane, the complete uninterrupted structure of a vascular relay was revealed (Fig. 6d). We next hypothesized that this distribution pattern of Cx43 in the vascular relay will promote coupling of the vascular cells along this region. As shown in Fig 6e–g, when a pericyte from a relay region was injected with Neurobiotin, the tracer spread much further than when a pericyte was targeted outside of the relay region. Moreover, the Neurobiotin labeling from a relay pericyte extended well into the intermediate and deep layers (compare Fig. 6e and f, bottom vertical views, and Fig. 6h). Interestingly, Neurobiotin spreading towards the major artery stopped abruptly at the artery. Thus, the vascular relay region has a distinct structural organization, potentially conferring an array of functional properties to this part of the vascular tree.

Cx37 plaques cover entire surface of the retinal vasculature.

In the superficial layer, Cx37 was associated with all regions of the vascular tree, as well as a number of what appeared to be ganglion cell neurons (Fig. 7a). In the high magnification images, Cx37 labeling coincided with DsRed protein in all vascular layers (Fig. 7b and c). All DsRed-positive mural cells expressed Cx37. In the artery, Cx37 puncta were found not only on DsRed-positive mural cells but also on PECAM-1 labeled endothelial cells (Fig. 8a–c). Similarly, capillaries and veins had expression of Cx37 in both mural and endothelial cells. In both vascular cell types, Cx37 positive puncta were not limited to the cellular

contacts and were evenly distributed on the entire surface of the cells. This distribution outside of the cellular contacts suggests that Cx37 may form hemichannels on the surface of the vascular cells. As we did not observe Neurobiotin spread from the surface of the vascular cells expressing Cx37, these hemichannels may normally remain closed, as was demonstrated for various hemichannels (for review see Good, Ek-Vitorin, & Burt, 2014; Goodenough & Paul, 2003).

Cx40 is predominantly expressed in the primary arteries at the endothelial cell contacts.

In the mouse retinal vasculature, Cx40 was localized to the primary arteries (Fig. 9a) similar to the expression pattern in the rat retina (Kuo et al., 2008). In the high magnification images, Cx40 was expressed in string-like structures, similar to Cx43 in relay regions. No Cx40 staining was detected in relays, veins, and capillaries of the superficial, intermediate, and deep layers (Fig. 9b–g). Weak Cx40 labeling was detected in some neurons of the GCL and some puncta in the inner retina (Fig. 9f and g). In the vasculature, Cx40 was colocalized with PECAM-1 (Fig. 9h–j), confirming its expression between the contacts of endothelial cells. The string-like pattern of Cx40 was reminiscent of Cx43 expression in the vascular relay. To probe coupling of the vascular cells in an artery, we injected an SMA cell with Neurobiotin (Fig. 9i). In contrast to an injected pericyte from a relay region, the Neurobiotin remained restricted to the targeted SMA-positive cell. These data suggest that under our experimental condition, SMA-positive cells were uncoupled in the artery.

GJs of endothelial cells closely colocalize with tight junctions of blood retina barrier.

Location of the Cx40 and Cx43 GJs at the membrane contacts between the endothelial cells provides a possibility for interaction between these GJs and other cell junction complexes such as adherens and tight junctions. To further explore this possibility, we triple-labeled a retina whole mount for a) Cx43, claudin5, and PECAM-1 or b) Cx40, claudin5, and PECAM-1 (Fig.10). Claudin5 was used as a marker of tight junctions (Nitta et al., 2003) and PECAM-1 was a marker of adherens proteins (Newman, 1997). Both Cx40 and Cx43 were studied at their occupied territories: primary arteries and relays, respectively. In both arteries and vascular relay regions, all connexin-positive strings were strictly colocalized with claudin5 (Fig. 10, arrows). In the fluorescent profiles, we found that the peaks of Cx40 and Cx43 coincided with and were proportional to the peaks of claudin5. In contrast, both connexin and claudin5 labeling did not precisely coincide with PECAM-1, and their peaks were disproportionate in size. The finest capillaries expressing comparable levels of claudin5 and PECAM-1, did not exhibit Cx40- and Cx43-positive strings (Fig. 10i–l). While the precise function for this arrangement is not clear, this colocalization of GJs and tight junctions may indicate a role for GJs in blood-retina barrier.

Discussion

In this work we characterized distinct distribution patterns of three major vascular connexins along the identified regions of the vascular tree. Specifically, we demonstrated that a) Cx43 was expressed in continuous string-like structures along the transition areas between the capillaries and arteries, termed “vascular relays”. On the cellular level, b) Cx43 was expressed in strings along endothelial cell contacts of vascular relays where it mediated

strong coupling among vascular cells -pericytes and endothelial cells. On the other hand, c) Cx37 puncta were associated with the entire surface of both mural and endothelial cells along the vascular tree. d) Cx40 expression was predominantly found on endothelial cells of the primary arteries. Interestingly, at their occupied territories, e) Cx43 and Cx40 clustered with tight junctions and, to a lesser extent, with adhesion contacts. Below, we will discuss the physiological implications of these findings in relation to vasomotor response and blood-retina barrier integrity.

Differential distribution of vascular gap junctions in the retina: structural basis for vascular domains.

The expression of GJs varied throughout the vascular tree and was associated with distinct functional domains. For example, Cx40 was located exclusively in endothelial cells of the primary arteries. In contrast, Cx43 was strongly expressed in the endothelial cells of the vascular relay region. Similar separation of connexins was described for rat aortic endothelium, where Cx40 was expressed in thoracic and abdominal endothelial cells and Cx43 in cells localized to the downstream edge of the ostia of branching vessels (Gabriels & Paul, 1998). Thus, Cx43 expression may be associated with zones of turbulent shear stress from disturbed blood flow. Indeed, when localized stress was induced by surgical coarctation of the aorta, it was sufficient to cause local upregulation of Cx43 (Gabriels & Paul, 1998). Thus, at different regions of the vascular tree, similar vascular cell types appeared to exhibit distinct GJ composition, suggesting functional specialization of the vascular domains.

It was noted previously that Cx40 and Cx43 are not co-expressed in the same cells and are not able to form a functional GJs between the neighboring cells (Bruzzone, Haefliger, Gimlich, & Paul, 1993; Elfgang et al., 1995; Haubrich et al., 1996). Interestingly, we found that Neurobiotin spread in the capillaries stopped abruptly at the artery. Similar Neurobiotin restriction was also noted in isolated rat vasculature (Oku et al., 2001) and assessed by measuring electrical conductances along the vascular tree (Puro, 2012). In contrast to the highly efficient transmission within capillaries and the arterioles, conductance dropped abruptly at the capillary/arteriole branch point. We demonstrated that this zone of Neurobiotin exclusion and drop of electric conductance coincided with the border between Cx43-positive endothelial cells of relay region and Cx40-positive endothelial cells of the artery. This suggests that the signal travelling through GJs along the vascular tree uses a non-GJ switch to get to the endothelium of the artery. Overall, our findings indicate that vascular cell communication is spatially regulated by selective expression of distinct connexins. As discussed further, this may serve a structural mechanism to control the extent of functional signaling along the vascular tree.

Signaling along vascular tree: the “vascular relay” region and its functional role.

In the retina, capillaries are strategically positioned in the synaptic layers to sense activities of surrounding neurons. On the other hand, the arteries placed outside of retinal synaptic layers are surrounded by smooth muscle cells and have a better capacity to adjust their diameter and blood flow than the capillaries with pericytes (Kornfield & Newman, 2014). Thus, the signal originated in capillaries may need to travel upstream towards the feeding

artery to produce there a stronger vasomotor response. While this spatial separation of the signal reception from the major vasomotor response element was also noted in various regions of the CNS (Iadecola, Yang, Ebner, & Chen, 1997; Kornfield & Newman, 2014; Rungta, Chaigneau, Osmanski, & Charpak, 2018), the structure mediating the signal propagation remained unclear. Here we describe a vascular relay region, a transition between the capillary and the feeding artery with a unique string-like expression of Cx43. Vascular cells along the relay exhibited the strongest Neurobiotin coupling, confirming functional connectivity. The Neurobiotin spread outside of vascular relays was limited. Furthermore, the pattern of Cx43-positive strings along the endothelial cell contacts and the Neurobiotin spread through endothelial cells suggest that the vascular signal propagates predominantly through endothelial cells. This is in agreement with electrical assessment of vascular connectivity. Specifically, Puro et al. have shown that the efficacy of radial transmission was 76% in the endothelial cells, contrasted to ~ 45% between pericytes and endothelial cells (Puro, 2012). Thus, most of the voltage generated by a pericyte is transmitted to the underlying endothelium, which then provides a pathway for proximal transmission. Similar results were obtained in other systems (arteries in hamster retractor muscle, (Emerson & Segal, 2000; Segal & Jacobs, 2001)).

Cx40 may perform a similar function in the arteries. Mice lacking Cx40 (Kirchhoff et al., 1998; Simon, Goodenough, & Paul, 1998) was shown to exhibit an impaired conduction of dilatory signals along arterioles. Spontaneous and irregular vasomotion was observed in a few Cx40-deficient mice, leading to arteriolar constriction and increased vascular resistance (de Wit et al., 2000). Together, these support a critical role for Cx40 in the propagation of arteriolar vasodilation.

GJs and the blood-tissue barrier properties.

In the current paper we determined precise co-localization of a tight junction protein claudin5 with Cx43 and Cx40. The precision of colocalization with claudin5 was much higher than that with an adherens protein, PECAM1. This suggests a possibility of interaction between GJs and tight junctions and a probable role of GJs in the blood-retina barrier. Accumulating evidence from the rodent models of diabetic retinopathy is consistent with our hypothesis. At the onset of diabetic retinopathy, downregulation of Cx43 (Bobbie et al., 2010; A. F. Li et al., 2003; Oku et al., 2001) preceded disruption of the blood-retina barrier and appearance of leaky blood vessels (Ivanova et al., 2017). Moreover, downregulation of Cx43 expression alone induced vascular cell death and promoted vascular permeability in the rat retina (Tien et al., 2014).

Association of GJs and tight junctions was also observed in other parts of the body. It has been shown that Cx40 and Cx43-containing GJs are required for endothelial barrier (Nagasawa et al., 2006). In porcine blood-brain barrier endothelial cells, Cx40 and Cx43-containing GJs co-precipitated with tight-junction proteins occludin, claudin5, and ZO-1. When GJs were pharmacologically blocked, the barrier properties of endothelial cells were inhibited leading to increased permeability of the blood vessels (Nagasawa et al., 2006). In the Sertoli cells of testis, Cx43 was transiently lost from the intercellular junctions during the spermiation process leading to an increase in vascular permeability. Cx43 re-associated

with the junctional proteins as soon as the barrier closes up again (Li, Mruk, Lee, & Cheng, 2010).

In conclusion, we determined domain-specific distribution of connexins along the vascular tree in the mouse retina. The functional implications of this specialized distribution will be addressed in future studies.

Acknowledgments:

This work was supported by NIH grants R01-EY026576 and R01-EY029796 (BTS). The authors thank Ms. Elizabeth Magier for comments on the manuscript.

References

Aarts E, Verhage M, Veenvliet JV, Dolan CV, & van der Sluis S (2014). A solution to dependency: using multilevel analysis to accommodate nested data. Nat Neurosci, 17(4), 491–496. doi: 10.1038/nn.3648 [PubMed: 24671065]

Akopian A, Atlasz T, Pan F, Wong S, Zhang Y, Volgyi B, … Bloomfield SA (2014). Gap junction-mediated death of retinal neurons is connexin and insult specific: a potential target for neuroprotection. J Neurosci, 34(32), 10582–10591. doi: 10.1523 [PubMed: 25100592]

Bloomfield SA, Xin D, & Osborne T (1997). Light-induced modulation of coupling between AII amacrine cells in the rabbit retina. Vis Neurosci, 14(3), 565–576. [PubMed: 9194323]

Bobbie MW, Roy S, Trudeau K, Munger SJ, Simon AM, & Roy S (2010). Reduced connexin 43 expression and its effect on the development of vascular lesions in retinas of diabetic mice. Invest Ophthalmol Vis Sci, 51(7), 3758–3763. doi: 10.1167/iovs.09-4489 [PubMed: 20130277]

Brisset AC, Isakson BE, & Kwak BR (2009). Connexins in vascular physiology and pathology. Antioxid Redox Signal, 11(2), 267–282. doi: 10.1089/ars.2008.2115 [PubMed: 18834327]

Brivanlou IH, Warland DK, & Meister M (1998). Mechanisms of concerted firing among retinal ganglion cells. Neuron, 20(3), 527–539. [PubMed: 9539126]

Bruzzone R, Haefliger JA, Gimlich RL, & Paul DL (1993). Connexin40, a component of gap junctions in vascular endothelium, is restricted in its ability to interact with other connexins. Mol Biol Cell, 4(1), 7–20. [PubMed: 8382974]

Campbell M, Nguyen AT, Kiang AS, Tam LC, Gobbo OL, Kerskens C, … Humphries P (2009). An experimental platform for systemic drug delivery to the retina. Proc Natl Acad Sci U S A, 106(42), 17817–17822. doi: 10.1073/pnas.0908561106 [PubMed: 19822744]

Carlson EC (1989). Fenestrated subendothelial basement membranes in human retinal capillaries. Invest Ophthalmol Vis Sci, 30(9), 1923–1932. [PubMed: 2777512]

Coombs J, van der List D, Wang GY, & Chalupa LM (2006). Morphological properties of mouse retinal ganglion cells. Neuroscience, 140(1), 123–136. doi: 10.1016/j.neuroscience.2006.02.079 [PubMed: 16626866]

Csaba G, Kovacs P, & Pallinger E (2006). EDAC fixation increases the demonstrability of biogenic amines in the unicellular Tetrahymena: a flow cytometric and confocal microscopic comparative analysis. Cell Biol Int, 30(4), 345–348. doi: 10.1016/j.cellbi.2005.12.011 [PubMed: 16530432]

Danesh-Meyer HV, Kerr NM, Zhang J, Eady EK, O'Carroll SJ, Nicholson LF, … Green CR (2012). Connexin43 mimetic peptide reduces vascular leak and retinal ganglion cell death following retinal ischaemia. Brain, 135(Pt 2), 506–520. doi: 10.1093/brain/awr338 [PubMed: 22345088]

Dang X, Doble BW, Kardami E (2003). The carboxy-tail of connexin-43 localizes to the nucleus and inhibits cell growth. Mol Cell Biochem, 242(1–2), 35–38. [PubMed: 12619863]

de Wit C, Roos F, Bolz SS, Kirchhoff S, Kruger O, Willecke K, & Pohl U (2000). Impaired conduction of vasodilation along arterioles in connexin40-deficient mice. Circ Res, 86(6), 649–655. [PubMed: 10747000]

Deans MR, Volgyi B, Goodenough DA, Bloomfield SA, & Paul DL (2002). Connexin36 is essential for transmission of rod-mediated visual signals in the mammalian retina. Neuron, 36(4), 703–712. [PubMed: 12441058]

Delaey C, & Van De Voorde J (2000). Regulatory mechanisms in the retinal and choroidal circulation. Ophthalmic Res, 32(6), 249–256. doi: 10.1159/000055622 [PubMed: 11015035]

Delorme B, Dahl E, Jarry-Guichard T, Briand JP, Willecke K, Gros D, & Theveniau-Ruissy M (1997). Expression pattern of connexin gene products at the early developmental stages of the mouse cardiovascular system. Circ Res, 81(3), 423–437. [PubMed: 9285645]

Denuc A, Nunez E, Calvo E, Loureiro M, Miro-Casas E, Guaras A, … Garcia-Dorado D, (2016). New protein-protein interactions of mitochondrial connexin 43 in mouse heart. J Cell Mol Med, 20(5), 794–803. doi: 10.1111/jcmm.12792 [PubMed: 26915330]

Durham JT, Dulmovits BM, Cronk SM, Sheets AR, & Herman IM (2015). Pericyte chemomechanics and the angiogenic switch: insights into the pathogenesis of proliferative diabetic retinopathy? Invest Ophthalmol Vis Sci, 56(6), 3441–3459. doi: 10.1167/iovs.14-13945 [PubMed: 26030100]

Elfgang C, Eckert R, Lichtenberg-Frate H, Butterweck A, Traub O, Klein RA, … Willecke K (1995). Specific permeability and selective formation of gap junction channels in connexin-transfected HeLa cells. J Cell Biol, 129(3), 805–817. [PubMed: 7537274]

Emerson GG, & Segal SS (2000). Endothelial cell pathway for conduction of hyperpolarization and vasodilation along hamster feed artery. Circ Res, 86(1), 94–100. [PubMed: 10625310]

Fang JS, Coon BG, Gillis N, Chen Z, Qiu J, Chittenden TW, … Hirschi KK (2017). Shear-induced Notch-Cx37-p27 axis arrests endothelial cell cycle to enable arterial specification. Nat Commun, 8(1), 2149. doi: 10.1038/s41467-017-01742-7 [PubMed: 29247167]

Fletcher EL, Hack I, Brandstatter JH, & Wassle H (2000). Synaptic localization of NMDA receptor subunits in the rat retina. J Comp Neurol, 420(1), 98–112. [PubMed: 10745222]

Furshpan EJ, & Potter DD (1957). Mechanism of nerve-impulse transmission at a crayfish synapse. Nature, 180(4581), 342–343. [PubMed: 13464833]

Gabriels JE, & Paul DL (1998). Connexin43 is highly localized to sites of disturbed flow in rat aortic endothelium but connexin37 and connexin40 are more uniformly distributed. Circ Res, 83(6), 636–643. [PubMed: 9742059]

Gastinger MJ, O'Brien JJ, Larsen NB, & Marshak DW (1999). Histamine immunoreactive axons in the macaque retina. Invest Ophthalmol Vis Sci, 40(2), 487–495. [PubMed: 9950609]

Gilula NB, Reeves OR, & Steinbach A (1972). Metabolic coupling, ionic coupling and cell contacts. Nature, 235(5336), 262–265. [PubMed: 4551177]

Good ME, Ek-Vitorin JF, & Burt JM (2014). Structural determinants and proliferative consequences of connexin 37 hemichannel function in insulinoma cells. J Biol Chem, 289(44), 30379–30386. doi: 10.1074/jbc.M114.583054 [PubMed: 25217644]

Goodenough DA, & Paul DL (2003). Beyond the gap: functions of unpaired connexon channels. Nat Rev Mol Cell Biol, 4(4), 285–294. doi: 10.1038/nrm1072 [PubMed: 12671651]

Gros DB, & Jongsma HJ (1996). Connexins in mammalian heart function. Bioessays, 18(9), 719–730. doi: 10.1002/bies.950180907 [PubMed: 8831288]

Guldenagel M, Sohl G, Plum A, Traub O, Teubner B, Weiler R, & Willecke K (2000). Expression patterns of connexin genes in mouse retina. J Comp Neurol, 425(2), 193–201. [PubMed: 10954839]

Guo R, Xu X, Lu Y, & Xie X (2017). Physiological oxygen tension reduces hepatocyte dedifferentiation in in vitro culture. Sci Rep, 7(1), 5923. doi: 10.1038/s41598-017-06433-3 [PubMed: 28724942]

Haefliger JA, Allagnat F, Hamard L, Le Gal L, Meda P, Nardelli-Haefliger D, … Alonso F (2017). Targeting Cx40 (Connexin40) Expression or Function Reduces Angiogenesis in the Developing Mouse Retina. Arterioscler Thromb Vasc Biol, 37(11), 2136–2146. doi: 10.1161/ATVBAHA.117.310072 [PubMed: 28982669]

Haefliger JA, Nicod P, & Meda P (2004). Contribution of connexins to the function of the vascular wall. Cardiovasc Res, 62(2), 345–356. doi: 10.1016/j.cardiores.2003.11.015 [PubMed: 15094354]

Haubrich S, Schwarz HJ, Bukauskas F, Lichtenberg-Frate H, Traub O, Weingart R, & Willecke K (1996). Incompatibility of connexin 40 and 43 Hemichannels in gap junctions between

mammalian cells is determined by intracellular domains. Mol Biol Cell, 7(12), 1995–2006. [PubMed: 8970160]

Haverkamp S, & Wassle H (2000). Immunocytochemical analysis of the mouse retina. J Comp Neurol, 424(1), 1–23. [PubMed: 10888735]

Hughes S, & Chan-Ling T (2004). Characterization of smooth muscle cell and pericyte differentiation in the rat retina in vivo. Invest Ophthalmol Vis Sci, 45(8), 2795–2806. doi: 10.1167/iovs.03-1312 [PubMed: 15277506]

Iadecola C, Yang G, Ebner TJ, & Chen G (1997). Local and propagated vascular responses evoked by focal synaptic activity in cerebellar cortex. J Neurophysiol, 78(2), 651–659. doi: 10.1152/jn.1997.78.2.651 [PubMed: 9307102]

Ivanova E, Kovacs-Oller T, & Sagdullaev BT (2017). Vascular Pericyte Impairment and Connexin43 Gap Junction Deficit Contribute to Vasomotor Decline in Diabetic Retinopathy. J Neurosci, 37(32), 7580–7594. doi: 10.1523/JNEUROSCI.0187-17.2017 [PubMed: 28674171]

Ivanova E, Toychiev AH, Yee CW, & Sagdullaev BT (2013). Optimized protocol for retinal wholemount preparation for imaging and immunohistochemistry. J Vis Exp(82), e51018. doi: 10.3791/51018 [PubMed: 24379013]

Ivanova E, Toychiev AH, Yee CW, & Sagdullaev BT (2014). Intersublaminar vascular plexus: the correlation of retinal blood vessels with functional sublaminae of the inner plexiform layer. Invest Ophthalmol Vis Sci, 55(1), 78–86. doi: 10.1167/iovs.13-13196 [PubMed: 24346172]

Ivanova E, Yee CW, Baldoni R Jr., & Sagdullaev BT (2016). Aberrant activity in retinal degeneration impairs central visual processing and relies on Cx36-containing gap junctions. Exp Eye Res, 150, 81–89. doi: 10.1016/j.exer.2015.05.013 [PubMed: 26005040]

Iwase T, Oveson BC, Hashida N, Lima e Silva R, Shen J, Krauss AH, … Campochiaro PA (2013). Topical pazopanib blocks VEGF-induced vascular leakage and neovascularization in the mouse retina but is ineffective in the rabbit. Invest Ophthalmol Vis Sci, 54(1), 503–511. doi: 10.1167/iovs.12-10473 [PubMed: 23169884]

Kawamura H, Sugiyama T, Wu DM, Kobayashi M, Yamanishi S, Katsumura K, & Puro DG (2003). ATP: a vasoactive signal in the pericyte-containing microvasculature of the rat retina. J Physiol, 551(Pt 3), 787–799. doi: 10.1113/jphysiol.2003.047977 [PubMed: 12876212]

Kotini M, Barriga EH, Leslie J, Gentzel M, Rauschenberger V, Schambony A, & Mayor R (2018). Gap junction protein Connexin-43 is a direct transcriptional regulator of N-cadherin in vivo. Nat Commun, 9(1), 3846. doi: 10.1038/s41467-018-06368-x [PubMed: 30242148]

Kerr NM, Johnson CS, de Souza CF, Chee KS, Good WR, Green CR, & Danesh-Meyer HV (2010). Immunolocalization of gap junction protein connexin43 (GJA1) in the human retina and optic nerve. Invest Ophthalmol Vis Sci, 51(8), 4028–4034. doi: 10.1167/iovs.09-4847 [PubMed: 20375327]

Kirchhoff S, Nelles E, Hagendorff A, Kruger O, Traub O, & Willecke K (1998). Reduced cardiac conduction velocity and predisposition to arrhythmias in connexin40-deficient mice. Curr Biol, 8(5), 299–302. [PubMed: 9501070]

Kong JH, Fish DR, Rockhill RL, & Masland RH (2005). Diversity of ganglion cells in the mouse retina: unsupervised morphological classification and its limits. J Comp Neurol, 489(3), 293–310. doi: 10.1002/cne.20631 [PubMed: 16025455]

Kornfield TE, & Newman EA (2014). Regulation of blood flow in the retinal trilaminar vascular network. J Neurosci, 34(34), 11504–11513. doi: 10.1523/JNEUROSCI.1971-14.2014 [PubMed: 25143628]

Kothmann WW, Massey SC, & O'Brien J (2009). Dopamine-stimulated dephosphorylation of connexin 36 mediates AII amacrine cell uncoupling. J Neurosci, 29(47), 14903–14911. doi: 10.1523/JNEUROSCI.3436-09.2009 [PubMed: 19940186]

Koulen P, Fletcher EL, Craven SE, Bredt DS, & Wassle H (1998). Immunocytochemical localization of the postsynaptic density protein PSD-95 in the mammalian retina. J Neurosci, 18(23), 10136–10149. [PubMed: 9822767]

Kuo IY, Chan-Ling T, Wojcikiewicz RJ, & Hill CE (2008). Limited intravascular coupling in the rodent brainstem and retina supports a role for glia in regional blood flow. J Comp Neurol, 511(6), 773–787. doi: 10.1002/cne.21873 [PubMed: 18925566]

Li AF, Sato T, Haimovici R, Okamoto T, & Roy S (2003). High glucose alters connexin 43 expression and gap junction intercellular communication activity in retinal pericytes. Invest Ophthalmol Vis Sci, 44(12), 5376–5382. [PubMed: 14638741]

Li MW, Mruk DD, Lee WM, & Cheng CY (2010). Connexin 43 is critical to maintain the homeostasis of the blood-testis barrier via its effects on tight junction reassembly. Proc Natl Acad Sci U S A, 107(42), 17998–18003. doi: 10.1073/pnas.1007047107 [PubMed: 20921394]

Makowski L, Caspar DL, Phillips WC, & Goodenough DA (1977). Gap junction structures. II. Analysis of the x-ray diffraction data. J Cell Biol, 74(2), 629–645. [PubMed: 889612]

Mastronarde DN (1983). Interactions between ganglion cells in cat retina. J Neurophysiol, 49(2), 350–365. doi: 10.1152/jn.1983.49.2.350 [PubMed: 6300342]

Meister M, Wong RO, Baylor DA, & Shatz CJ (1991). Synchronous bursts of action potentials in ganglion cells of the developing mammalian retina. Science, 252(5008), 939–943. [PubMed: 2035024]

Nagasawa K, Chiba H, Fujita H, Kojima T, Saito T, Endo T, & Sawada N (2006). Possible involvement of gap junctions in the barrier function of tight junctions of brain and lung endothelial cells. J Cell Physiol, 208(1), 123–132. doi: 10.1002/jcp.20647 [PubMed: 16547974]

Newman PJ (1997). The biology of PECAM-1. J Clin Invest, 99(1), 3–8. doi: 10.1172/JCI119129 [PubMed: 9011572]

Nitta T, Hata M, Gotoh S, Seo Y, Sasaki H, Hashimoto N, … Tsukita S, (2003). Size-selective loosening of the blood-brain barrier in claudin-5-deficient mice. J Cell Biol, 161(3), 653–660. doi: 10.1083/jcb.200302070 [PubMed: 12743111]

Oku H, Kodama T, Sakagami K, & Puro DG (2001). Diabetes-induced disruption of gap junction pathways within the retinal microvasculature. Invest Ophthalmol Vis Sci, 42(8), 1915–1920. [PubMed: 11431461]

Pitts JD, & Simms JW (1977). Permeability of junctions between animal cells. Intercellular transfer of nucleotides but not of macromolecules. Exp Cell Res, 104(1), 153–163. [PubMed: 836400]

Puro DG (2012). Retinovascular physiology and pathophysiology: new experimental approach/new insights. Prog Retin Eye Res, 31(3), 258–270. doi: 10.1016/j.preteyeres.2012.01.001 [PubMed: 22333041]

Ribelayga C, Cao Y, & Mangel SC (2008). The circadian clock in the retina controls rod-cone coupling. Neuron, 59(5), 790–801. doi: 10.1016/j.neuron.2008.07.017 [PubMed: 18786362]

Ripps H (2002). Cell death in retinitis pigmentosa: gap junctions and the ‘bystander’ effect. Exp Eye Res, 74(3), 327–336. doi: 10.1006/exer.2002.1155 [PubMed: 12014914]

Rungta RL, Chaigneau E, Osmanski BF, & Charpak S (2018). Vascular Compartmentalization of Functional Hyperemia from the Synapse to the Pia. Neuron, 99(2), 362–375 e364. doi: 10.1016/j.neuron.2018.06.012 [PubMed: 29937277]

Schallek J, Geng Y, Nguyen H, & Williams DR (2013). Morphology and topography of retinal pericytes in the living mouse retina using in vivo adaptive optics imaging and ex vivo characterization. Invest Ophthalmol Vis Sci, 54(13), 8237–8250. doi: 10.1167/iovs.13-12581 [PubMed: 24150762]

Schneeweis DM, & Schnapf JL (1995). Photovoltage of rods and cones in the macaque retina. Science, 268(5213), 1053–1056. [PubMed: 7754386]

Segal SS, & Jacobs TL (2001). Role for endothelial cell conduction in ascending vasodilatation and exercise hyperaemia in hamster skeletal muscle. J Physiol, 536(Pt 3), 937–946. [PubMed: 11691885]

Simon AM, Goodenough DA, & Paul DL (1998). Mice lacking connexin40 have cardiac conduction abnormalities characteristic of atrioventricular block and bundle branch block. Curr Biol, 8(5), 295–298. [PubMed: 9501069]

Slavi N, Toychiev AH, Kosmidis S, Ackert J, Bloomfield SA, Wulff H, … Srinivas M (2018). Suppression of connexin 43 phosphorylation promotes astrocyte survival and vascular regeneration in proliferative retinopathy. Proc Natl Acad Sci U S A, 115(26), E5934–E5943. doi: 10.1073/pnas.1803907115 [PubMed: 29891713]

Sohl G, & Willecke K (2004). Gap junctions and the connexin protein family. Cardiovasc Res, 62(2), 228–232. doi: 10.1016/j.cardiores.2003.11.013 [PubMed: 15094343]

Tien T, Muto T, Barrette K, Challyandra L, & Roy S (2014). Downregulation of Connexin 43 promotes vascular cell loss and excess permeability associated with the development of vascular lesions in the diabetic retina. Mol Vis, 20, 732–741. [PubMed: 24940027]

Tornqvist K, Yang XL, & Dowling JE (1988). Modulation of cone horizontal cell activity in the teleost fish retina. III. Effects of prolonged darkness and dopamine on electrical coupling between horizontal cells. J Neurosci, 8(7), 2279–2288. [PubMed: 3249225]

Toychiev AH, Ivanova E, Yee CW, & Sagdullaev BT (2013). Block of gap junctions eliminates aberrant activity and restores light responses during retinal degeneration. J Neurosci, 33(35), 13972–13977. doi: 10.1523 [PubMed: 23986234]

Volgyi B, Kovacs-Oller T, Atlasz T, Wilhelm M, & Gabriel R (2013). Gap junctional coupling in the vertebrate retina: variations on one theme? Prog Retin Eye Res, 34, 1–18. doi: 10.1016/j.preteyeres.2012.12.002 [PubMed: 23313713]

Watanabe A (1958). The interaction of electrical activity among neurons of lobster cardiac ganglion. Jpn J Physiol, 8(4), 305–318. [PubMed: 13620382]

Weidmann S (1969). Electrical coupling between myocardial cells. Prog Brain Res, 31, 275–281. doi: 10.1016/S0079-6123(08)63246-X [PubMed: 4900114]

Wilhelm K, Happel K, Eelen G, Schoors S, Oellerich MF, Lim R, … Potente M (2016). FOXO1 couples metabolic activity and growth state in the vascular endothelium. Nature, 529(7585), 216–220. doi: 10.1038/nature16498 [PubMed: 26735015]

Yanagida K, Liu CH, Faraco G, Galvani S, Smith HK, Burg N, … Hla T (2017). Size-selective opening of the blood-brain barrier by targeting endothelial sphingosine 1-phosphate receptor 1. Proc Natl Acad Sci U S A, 114(17), 4531–4536. doi: 10.1073/pnas.1618659114 [PubMed: 28396408]

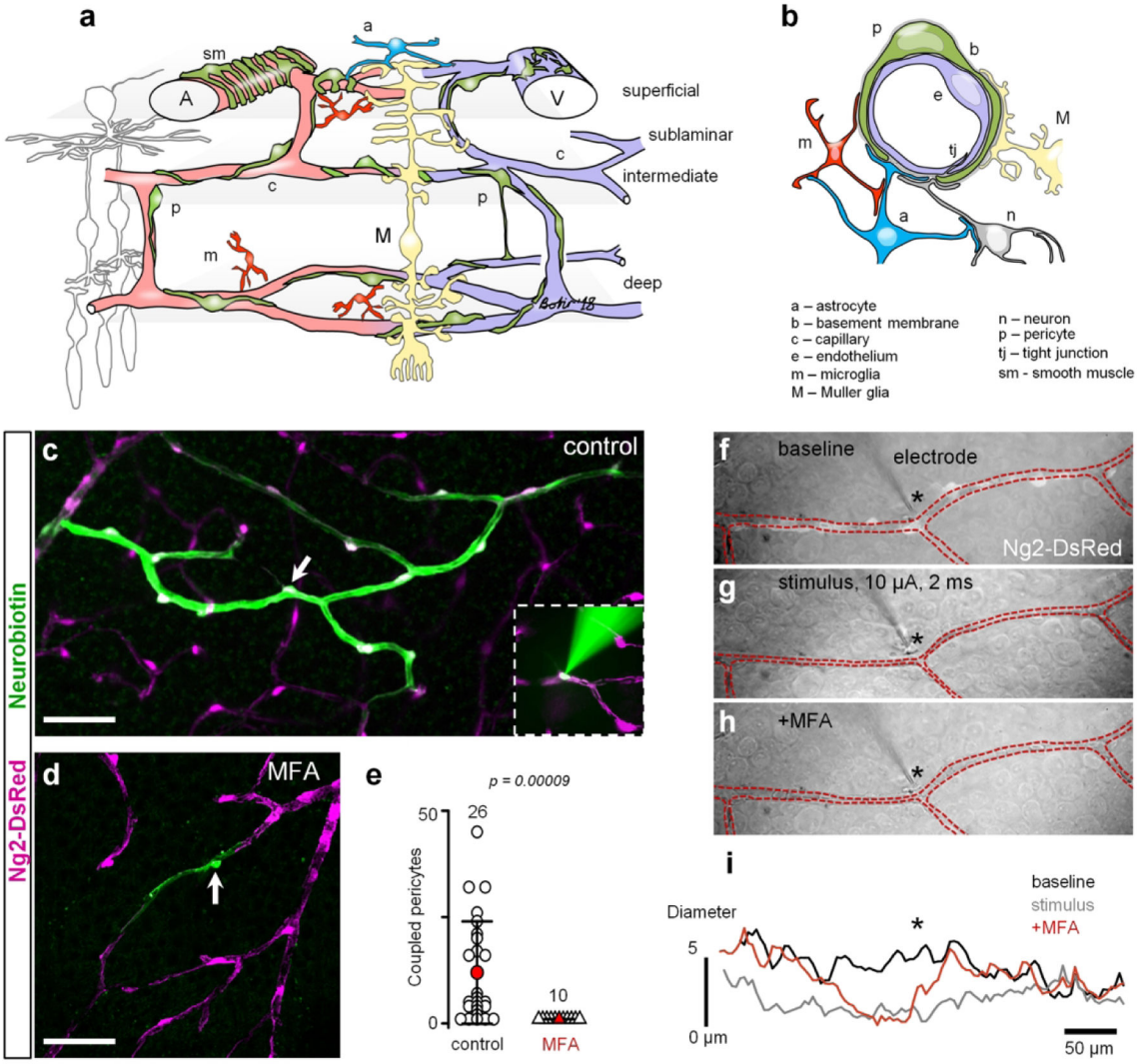

Figure 1. GJs mediate intercellular communication and propagation of vasomotor response.

(a) Specialized domains of the vascular tree. (b) Cross-section of the neurovascular unit. (c) In the living retina whole mount of NG2-DsRed mice, in which all contractile vascular cells express DsRed (magenta), Neurobiotin (green) injected into a single pericyte (arrow) spread to neighboring vascular cells through GJs. Inset shows electroporation procedure. (d) In the presence of pan-GJ blocker meclofenamenic acid (MFA, 50 µM), Neurobiotin spread was limited to the injected pericyte (arrow). (e) Quantification of the Neurobiotin spread in control and in the presence of MFA shows that under normal conditions, vascular cells are extensively coupled through GJs (data are shown as average ± SD; control: 11.96 ± 12, 26 samples, 15 mice; MFA: 1.0 ± 0.01, 10 samples, 8 mice; T-test, p = 0.00009). (f–h) Under physiological conditions, stimulation of an individual pericyte (identified based on NG2-DsRed labeling, white cells along blood vessel in the top panel) led to constriction of the capillary and to spreading of the constriction to the neighboring regions beyond the processes of the simulated pericyte. In the presence of MFA, stimulation of a pericyte led to vasoconstriction underneath the stimulated pericyte, but did not propagate to the neighboring

regions. (i) Quantification of the vasoconstriction and propagation of the vasomotor response determined that GJs mediate propagation of the signal along the capillary and they were not involved in vasoconstriction of the stimulated pericyte. Scale bar 50 μm.

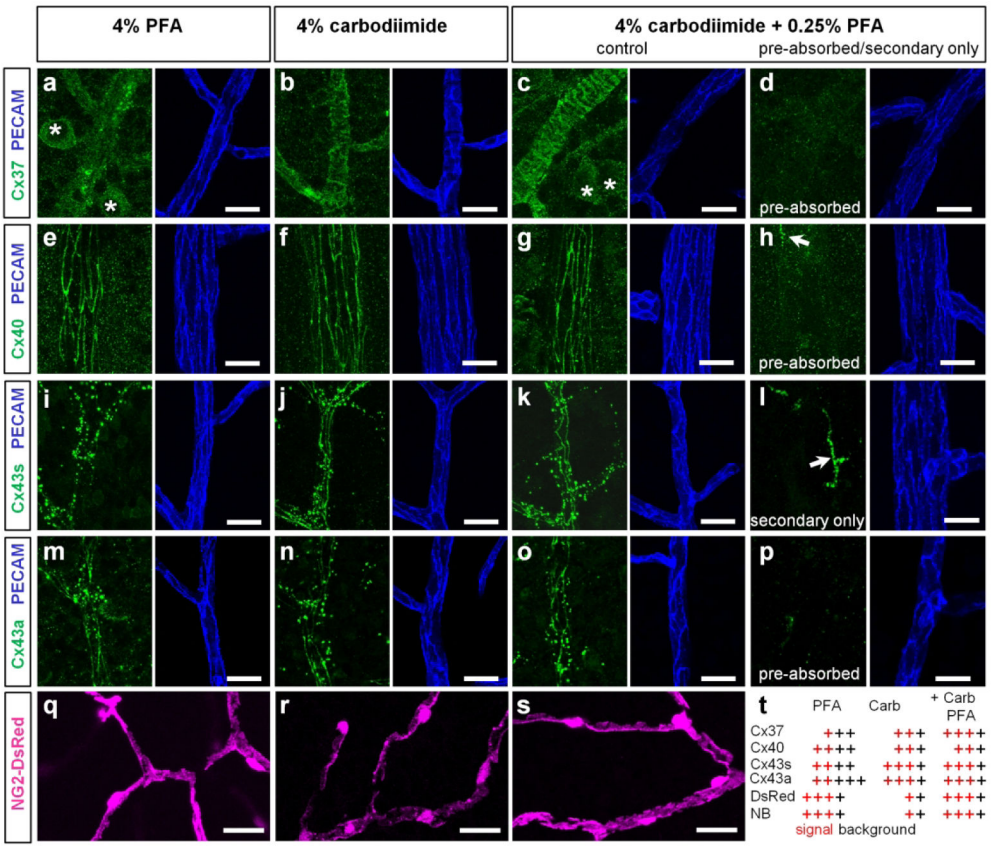

Figure 2. Validation and optimization of Connexin antibodies used in this study.

(a–d) Cx37 labeling revealed just a few puncta (green) on blood vessels (blue) in pure PFA fixative (a) and entire outlines of contractile cells in carbodiimide-based fixatives (b and c). Ganglion cells were more visible in PFA fixative (asterisks); the lowest background was in carbodiimide. Pre-absorption of the antibody with a control peptide eliminated the labeling (d). (e–h) Cx40 (green) was associated with outlines of endothelial cells (blue) in all fixative with the less background in carbodiimide (f). Incubation of primary antibody eliminated the labeling (h) with the exception of labeled microglia (arrow). (i–k) Cx43s-positive puncta (green, Sigma antibody) were associated with vasculature in PFA fixative (i); in addition string-like structures along endothelial cell contacts (blue) became visible in carbodiimide fixative (j–k). (l) Omission of the primary antibody eliminated punctate and string-like structures; the microglia was labeled by the secondary antibody (arrow). (m–p) Cx43a produced identical pattern as Cx43s in carbodiimide containing fixatives (n, o). In pure PFA fixative, this antibody labeled well punctate and string-like structures; however the background was significantly higher (m). Incubation of the primary antibodies with control peptide eliminated the specific labeling (p). (q–s) Morphology of DsRed expressing pericytes was best preserved in PFA-containing fixatives (q and s); the DsRed labeling in pericyte processes was lost in pure carbodiimide fixative (q). (t) Summary of fixation procedure. Red crosses indicate signal, black crosses – background; the number of crosses indicates intensity. Scale bar 10 μm. Cx43s – Cx43 antibody from Sigma, Cx43a – Cx43 antibody from Alomone, NB – Neurobiotin.

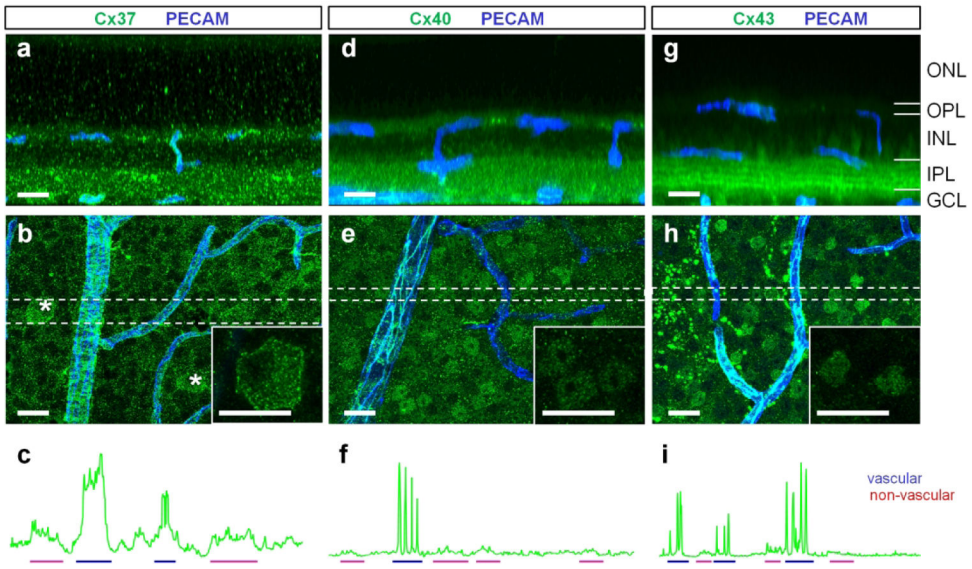

Figure 3. Cx37, Cx40, and Cx43 are expressed in retinal neurons at much lower levels than in the vasculature.

(a) Cx37 expression shown in a vertical view, created by rotation of a z-stack from the corresponding retinal whole mount region in (b). (b) Confocal projection of a retinal whole mount at the GCL. Some ganglion cells expressed Cx37 at their cell membrane (asterisks, insert). (c) Blood vessels had higher expression of Cx37 (blue) than ganglion cells (red). (d–e) Cx40 was weakly expressed in numerous nuclei of inner retinal neurons. High expression of Cx40 was detected in blood vessels (f, blue). (g–i) Cx43 was expressed in nuclei (insert) and processes of inner retinal neurons (g, four bright bands in the inner plexiform layer). The expression in neurons was lower than in blood vessels (i). Scale bar 20 μm. ONL – outer nuclear layer, OPL – outer plexiform layer, INL – inner nuclear layer, IPL – inner plexiform layer, GCL – ganglion cell layer.

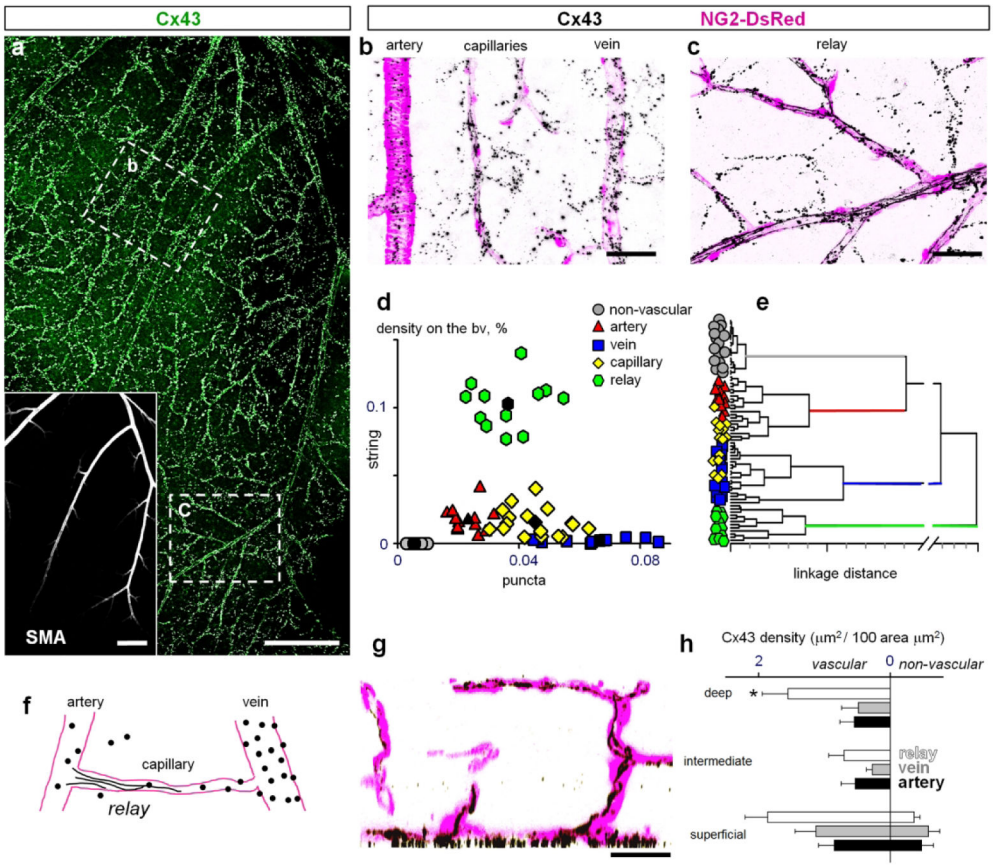

Figure 4. Hierarchy within the vascular tree dictates distinct patterns of Cx43 clustering.

(a) Cx43 is highly concentrated along retinal vasculature. Inset shows the arteries from the same area labeled for smooth muscle actin (SMA). Scale bar 200 µm. (b) In the superficial layer from area b in (a), majority of puncta were associated with vasculature: arteries, veins and capillaries and lower number of similar size puncta were present outside of the blood vessels. Scale bar 50 µm. (c) In the branches of major arteries from an area similar to the area c in (a), string-like structures running along the blood vessels were found in addition to the puncta. Scale bar 50 µm. (d) Density of the Cx43 puncta was the highest on veins and capillaries. The strings were found predominantly in relay regions connecting artery with capillaries. Density of Cx43 puncta outside of the blood vessels was significantly lower and no strings were detected. (e) Dendrogram created by cluster analysis of data from (d). (f) Schematic presentation of Cx43 expression pattern in retinal vasculature. (g) In a vertical section through the retina (created by rotation of a thin slit from the z-stack), the string-like structures from the superficial layer were extending along some capillaries into the intermediate and deep vascular layers. Scale bar 50 µm. (h) Distribution of Cx43 shows that Cx43 (puncta and strings combined) is predominantly expressed on the vasculature throughout the retina. The relays have the highest densities of Cx43-positive structures. The intermediate and deep layer capillaries above these relay zones also have the highest expression of Cx43 in string-like structures. The non-vascular expression in the superficial layer reflects the puncta outside of the blood vessels; no puncta of the same size and labeling intensity was detected in the intermediate and deep layers. Data are shown as average ± SD;

arteries, vein and transitions were quantified in 6 samples from 6 mice; capillaries and non-vascular areas in n = 12 samples from n = 6 mice. ANOVA on ranks, * p = 0.0001.

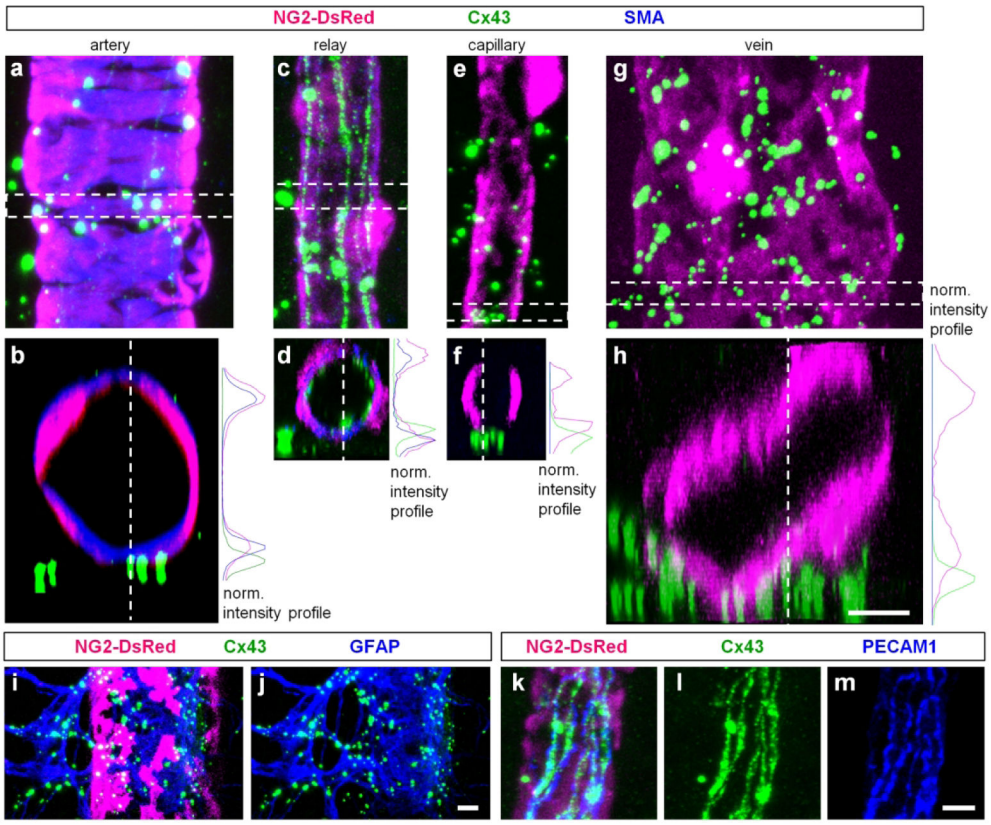

Figure 5. Cx43 is primarily localized to astrocytes and vascular cells.

(a) Around an artery, majority of the large puncta was not directly associated with vascular cells. (b) A vertical view from the highlighted area in (a) was obtained by 90^0 rotation of the z-stack. On the right, fluorescence intensity profile for the three labeling from (b). (c–d) In the relay, large puncta were also not directly located on the blood vessels contrarily to the string-like structures which were enclosed by the mural cells (d panel and the intensity profile). (e–f) Around the finest capillaries, Cx43-puncta were mostly outside of the blood vessels. (h) In veins, putative labeling was not directly associated with mural cells. (i–j) Bright Cx43 puncta around blood vessels were localized to astroglia labeled for glial fibrillary acidic protein (GFAP). (k–m) Cx43-positive strings were associated with endothelial cells labeled for platelet endothelial cell adhesion molecule-1 (PECAM-1). Scale bar 5 μm.

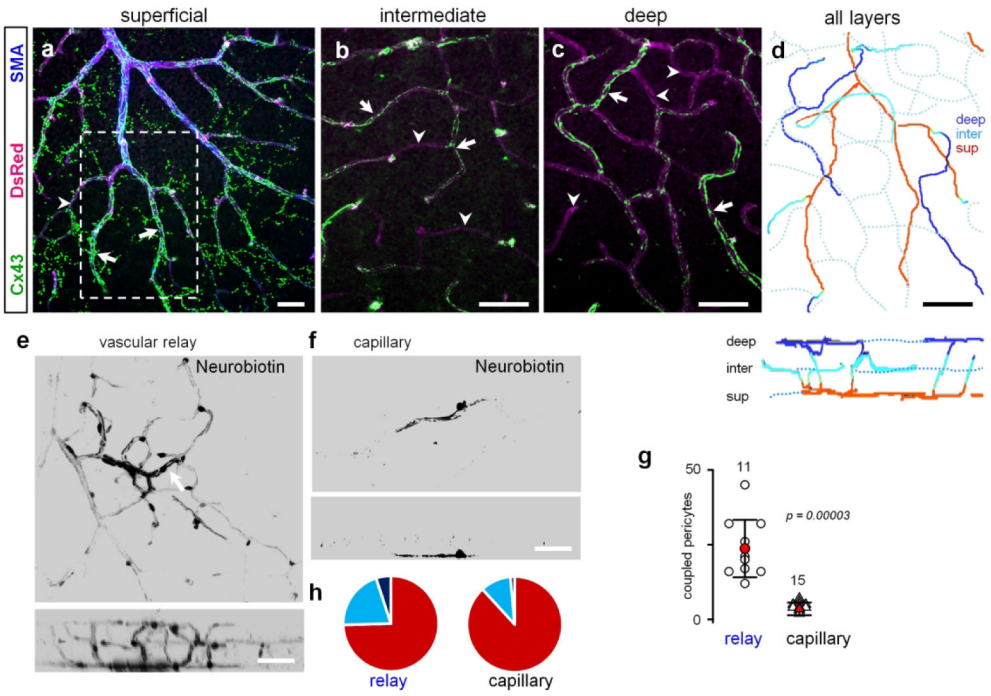

Figure 6. Cx43 promotes vascular coupling between the capillaries and the artery.

(a-c) The relay zones were identified based on the staining against smooth muscle actin (SMA). The string-like Cx43-positive structures started at the primary artery and continued uninterrupted beyond SMA-labeling into selected capillaries (arrows). Some capillaries had much weaker or no string-like expression (arrowheads). The strings from the superficial layer in (a) extended into intermediate (b) and deep (c) vascular layer capillaries using the shortest route from the artery. Scale bar 50 μm. (d) In the projection of all layers, string-bearing selected capillaries created a specialized vascular domain – vascular relay - spanning all three layers. The bottom panel shows a vertical view. Scale bar 50 μm. (e) Neurobiotin injected into a pericyte (arrow) in relay area spread throughout the large area. (f) Neurobiotin injected into the area outside the relay was restricted to a few pericytes. (g) Quantification shows that under normal conditions cells are extensively coupled through GJs in vascular relay (data are shown as average ± SD; standard: 3.3 ± 2.1, 15 samples, 8 mice; sensor: 23.7 ± 9.6, 11 samples, 6 mice; T-test, p = 0.00003). (h) Distribution of Cx43-positive strings across vascular layers shows that in the vascular relay region Neurobiotin spread farther into intermediate and deep vascular layers.

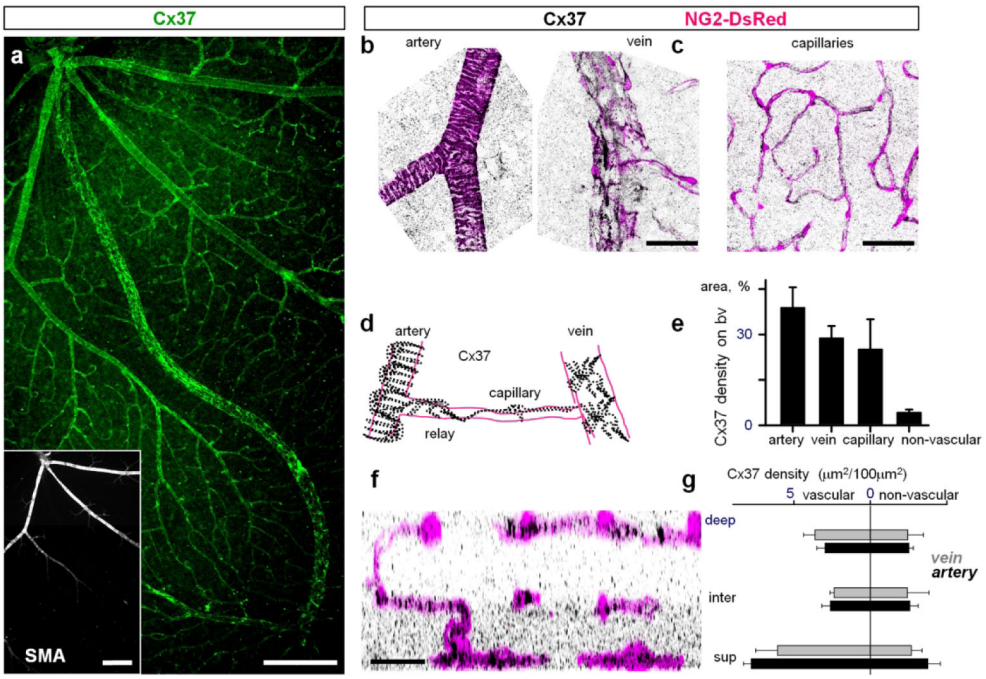

Figure 7. Cx37 is expressed in mural cells.

(a) Cx37 was located on all types of blood vessels in a retina whole mount. Insert identifies arteries based on the presence of smooth muscle actin labeling (SMA). Scale bar 200 µm. (b–c) In high magnification contractile cells identified by DsRed labeling express Cx37. (d) Schematic presentation of Cx37 distribution on retinal vasculature. (e) Cx37 density was high on all types of vasculature. (f) Cx37 distribution in a vertical retinal view shows punctate labeling in the inner plexiform layer. (g) Density of Cx37-labeled structures in all vascular layers. Scale bar 50 µm.

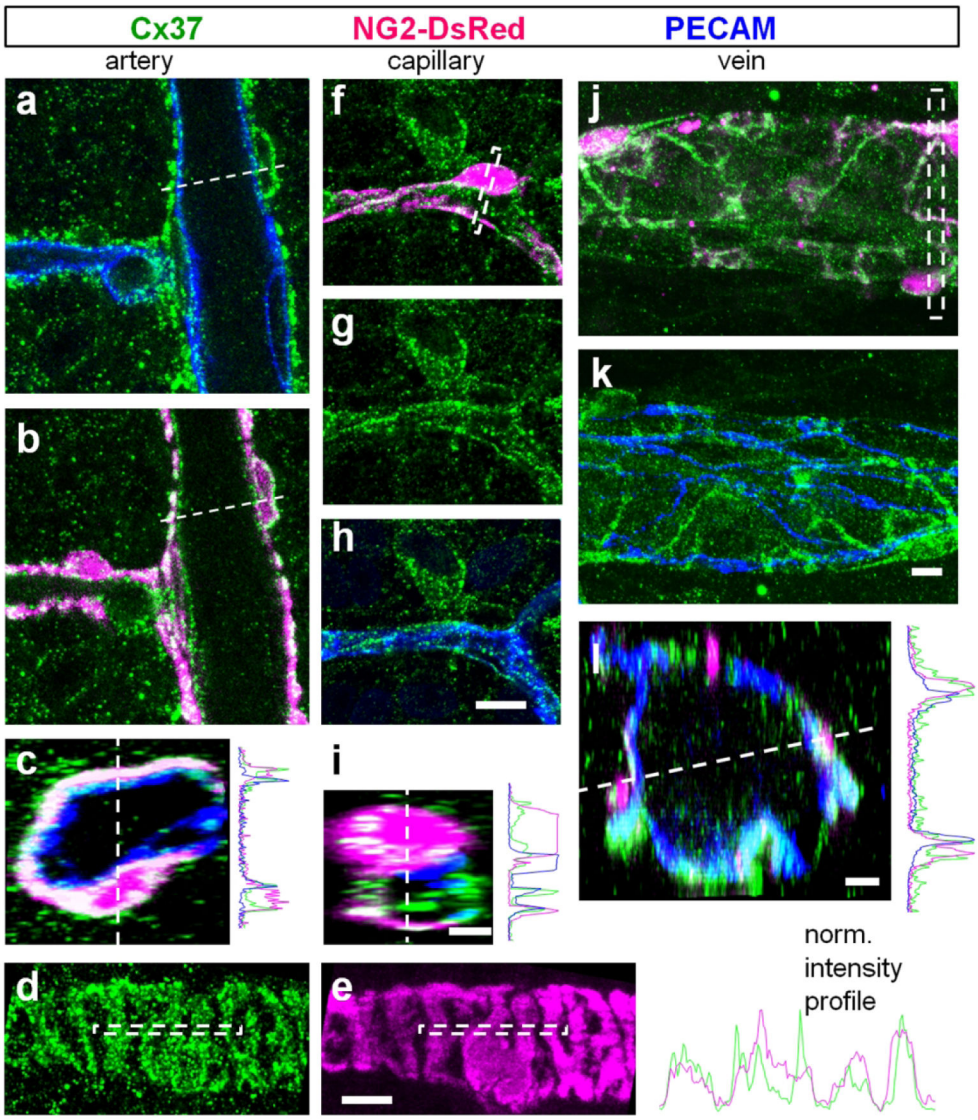

Figure 8. Cx37 is expressed in all vascular cells.

(a) In confocal section through an artery, puncta of cx37 (green) were present on endothelial cells (blue). (b) In the same artery, Cx37 was also co-localized on mural cells (magenta). (c) In the cross section of the artery from (a-b) Cx37 was present on both endothelial and contractile cells as reflected by the intensity profile on the right. (d–e) Cx37 was present on the entire membrane of the mural cells. (f–i) Similar to artery, in a capillary Cx43 was expressed in both endothelial and contractile cells. (j–I) In veins the strongest Cx37 labeling was around pericytes. Cx37 puncta were present on endothelial cells. Scale bar 5 μm.

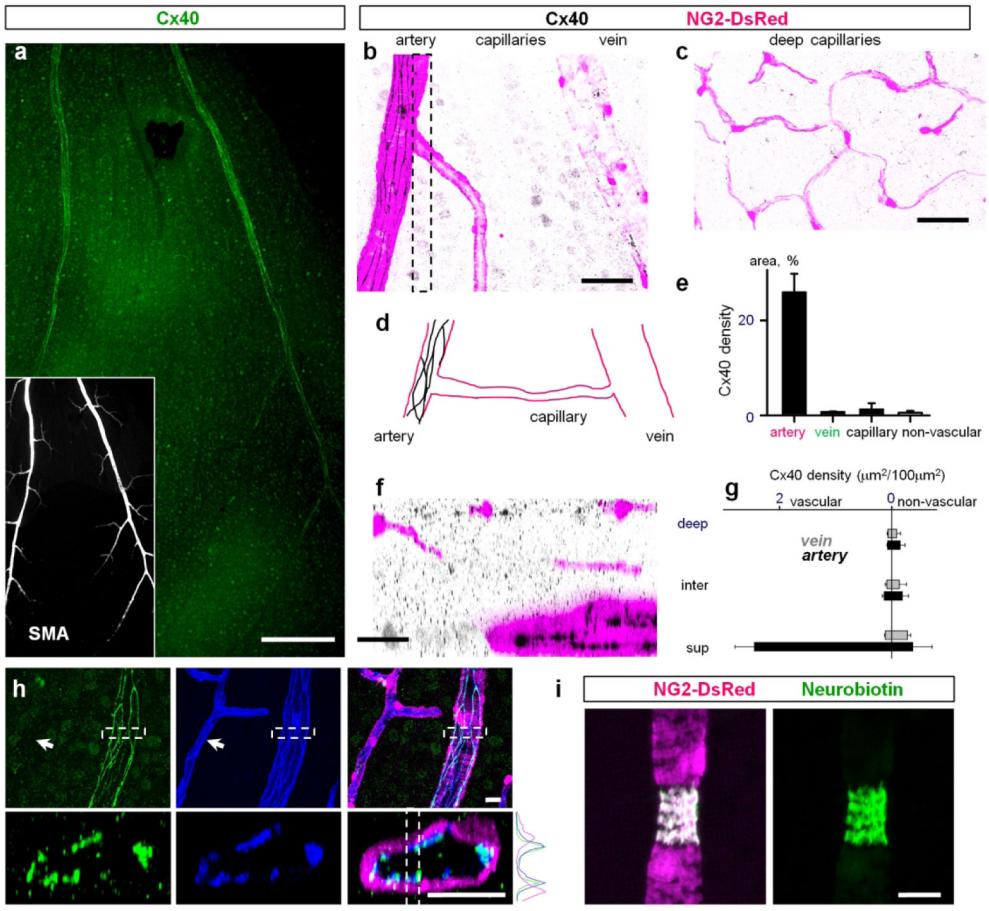

Figure 9. Cx40 was primarily localized to endothelial cells of the primary arteries.

(a) Cx40 was associated with primary arteries and some neurons in the ganglion cell layer of the retina whole mount. Insert shows primary arteries labeled for smooth muscle actin (SMA). Scale bar 200 µm. (b) In a high magnification of the superficial vascular layer Cx40 was localized directly to arteries. Scale bar 50 µm. (c) Cx40 was not detected in neither intermediate layer nor deep layer capillaries. Scale bar 50 µm. (d) Schematic presentation of Cx40 distribution in the superficial layer. (e) Quantification of Cx40 distribution on blood vessels of the superficial layer. (f) Vertical view of the confocal z-stack through the area highlighted in (b). Scale bar 25 µm. (g) Density of Cx40 in vascular layers. (h–j) Cx40 was colocalized on endothelial cells of the primary arteries but not on the capillaries (arrow). (i) Neurobiotin injected into a smooth muscle cell did not propagate to neighboring vascular cells. Please note that the targeted SMA-positive cell constricted during Neurobiotin injection. Scale bar 25 µm.

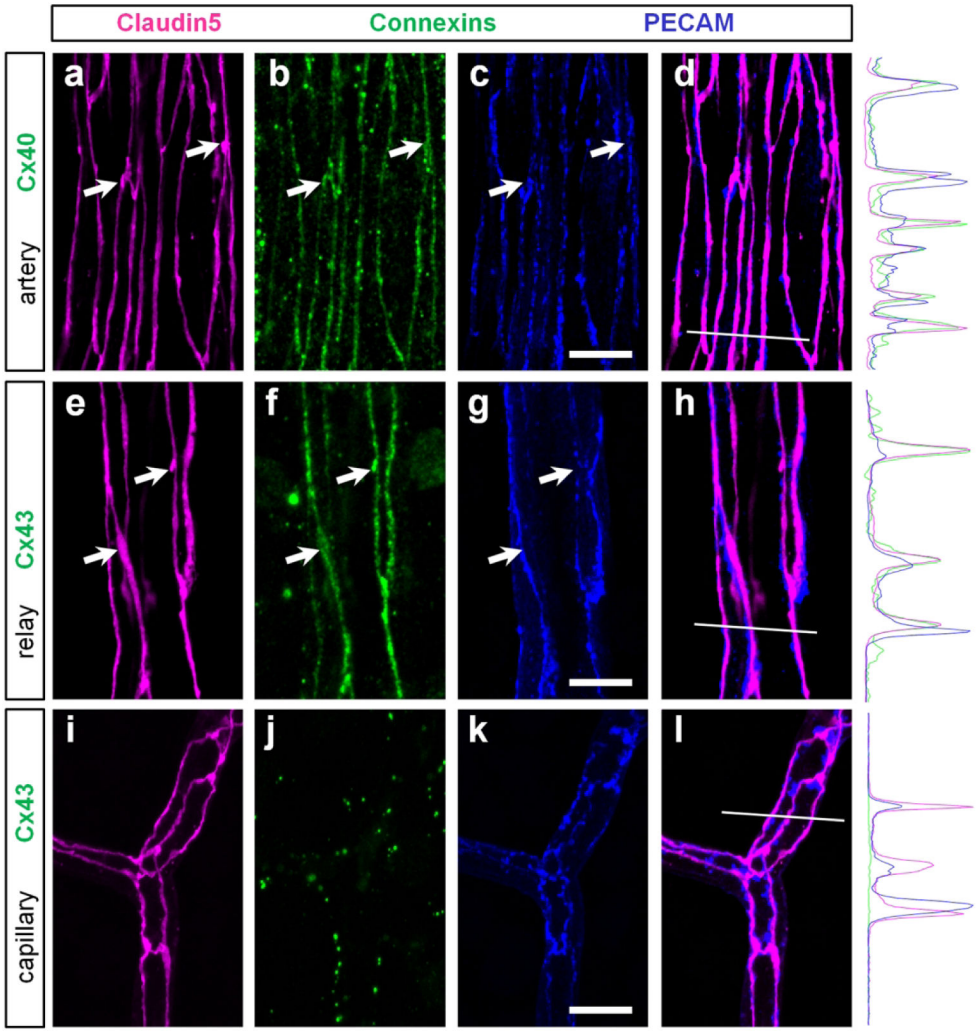

Figure 10. In the arteries and relays gap junctions of endothelial cells strictly colocalize with tight junctions.

(a–d) In the artery, Cx40 (green) was strictly colocalized with tight junctions (magenta, arrows) and less precisely with adherens proteins (blue). In a merged image of claudin5 and PECAM (d), the colocalization was not precise. White line highlights the region used for fluorescent intensity profile. Note that claudin5 and Cx40 profiles closely match and differ from the PECAM profile. (e–h) In the vascular relay, Cx43-positive strings were colocalized with tight junctions including strings and small varicosities (arrows). (i–l) In the capillary, Cx43 was not detected along tight junctions. Scale bar 10 μm.

Table 1.

Primary antibodies

Molecular marker	Immunogen	Host	Dilution	Clone	Source	RRID
Albumin	whole mouse albumin	goat	1:800	poly	Bethyl, A90–234A	RRID:AB_67122
claudin5 clone 4C3C2, Alexa488	Synthetic peptide from the mouse claudin5	mouse	1:10000	mono	Invitrogen, 352588	RRID:AB_2532189
Connexin 43 (Cx43s)	PSSRASSRASSRPRPDDLEI	rabbit	1:2000	poly	Sigma, C6219	RRID:AB_476857
Connexin 43 (Cx43a)	(C)HAQPFDFPDDNQNSK	rabbit	1:10000	poly	Alomone, ACC-201	RRID:AB_10917597
Connexin 40	(C)GHRFPQGYHSDKR	rabbit	1:3000	poly	Alomone, ACC-205	RRID:AB_2340916
Connexin 37	(C)EHQMAKISVAEDGR	rabbit	1:2000	poly	Alomone, ACC-204	RRID:AB_2722598
Smooth muscle actin, SMA, 1A4	N-terminal synthetic decapeptide of α-SMA	mouse	1:1000	mono	Sigma, A5228	RRID:AB_262054
Glial fibrillary acidic protein, GFAP	purified bovine GFAP	chicken	1:3000	poly	Millipore, AB5541	RRID:AB_177521
CD31/PECAM-1	Mouse myeloma cell NS0-derived recombinant mouse CD31 Glu18-Lys590	goat	1:6000	poly	RD, AF3628	RRID:AB_2161028